Politecnico di Milano
I Engineering Major
Environmental and Land Planning Engineering

HYDRO-MECHANICAL BEHAVIOUR OF A HIGH DENSITY COMPACTED BENTONITE FOR ITS IMPLEMENTATION IN GEOLOGICAL DISPOSAL OF NUCLEAR WASTE

Supervisor:
D.V. STERPI

Co-supervisors:
R. CHARLIER
F. COLLIN
A.C. DIEUDONNE

Candidate:
SARA ROZZONI
819935

Academic Year 2014-2015

HYDRO-MECHANICAL BEHAVIOUR OF A HIGH DENSITY COMPACTED BENTONITE FOR ITS IMPLEMENTATION IN GEOLOGICAL DISPOSAL OF NUCLEAR WASTE

Sara Rozzoni

April 8, 2016

Contents

List of Figures

List of Tables

Abstract

High density compacted bentonite is the most suitable material as sealing and backfilling buffer in the geological nuclear waste disposal, thanks to its physico-chemical, hydraulic and mechanical characteristics. In particular, its low permeability and its swelling capacity when hydrated make it the best option so far.
Some experimental tests have been performed on a specific bentonite, in various conditions: powder, liquid, plastic and compacted. The aim was initially to characterise it and to look for some similarities with literature data. An X-Ray Diffraction allowed to detect the mineralogical composition of the studied bentonite. Then, its grain and pore size distributions have been estimated respectively from a sedimentation and sieve analysis, and from a Mercury Intrusion Porosimetry which showed a decrease in macropores for increasing dry density. The Atterberg limits have been experimentally determined. The experimental findings, which led to reliable results, show a similarity between the bentonite under consideration and the commercialised MX-80 bentonite, for most of the parameters.
The hydraulic properties have been studied as well. The soil-water retention curve of the compacted material has been assessed by applying the vapour equilibrium technique; it has also shown an anisotropic behaviour in axial and lateral swelling. The permeability value has been estimated both from a falling head test and from an oedometric consolidation test; the latter one has given a more reliable value, close to the one accepted by the literature.
In order to characterise the volume change of the studied bentonite upon hydration, four swelling tests have been performed at the oedometer: they detected an exponential increase of the swelling pressure with the compacted material dry density.
Finally, the bentonite behaviour has been modelled through a hydro-mechanical coupled model, implemented in the finite element code LAGAMINE. A specific constitutive model has been calibrated on the observed material behaviour: the Barcelona Basic Model, with the appropriate parameters, is able to reproduce it satisfactorily.

Sommario

La bentonite compattata ad alte densità rappresenta il materiale più adatto da impiegare come barriera ingegneristica nelle opere di smaltimento sotterraneo di scorie nucleari, grazie alle sue caratteristiche fisico-chimiche, idrauliche e meccaniche. La sua bassa permeabilità e la sua capacità di rigonfiamento sotto idratazione la rendono a oggi l'opzione migliore.
Alcuni test sperimentali sono stati eseguiti su una specifica bentonite. Obiettivo di questi test era caratterizzare la bentonite e confrontarla con i materiali già in commercio. Una diffrazione a raggi X ne ha determinato la composizione mineralogica; la sua distribuzione granulometrica e porosimetrica è stata stimata rispettivamente da un'analisi granulometrica per setacciatura e sedimentazione, e da una porosimetria a intrusione di mercurio, che ha mostrato un decremento della macroporosità con l'aumento di densità secca. Anche i limiti di Atterberg sono stati determinati sperimentalmente.
Alla luce dei risultati ottenuti da questi test, che possono essere considerati affidabili, é stato possibile cogliere una somiglianza con la bentonite in commercio MX-80.
Per quanto riguarda il comportamento idraulico, la curva di ritenzione idrica è stata determinata tramite la tecnica di equilibrio di vapore, che ha anche evidenziato un'anisotropia di rigonfiamento in direzione assiale e trasversale. La permeabilità è stata stimata tramite un test a carico variabile e un test di consolidazione edometrica; il secondo ha fornito il valore più accettabile, prossimo a quelli proposti dalla letteratura.
Sono stati eseguiti quattro test di rigonfiamento con edometro, al fine di studiare le capacità espansive della bentonite analizzata: i dati mostrano una crescita esponenziale della pressione di rigonfiamento con la densità secca del materiale.
Infine, il suo comportamento è stato studiato con un modello idro-meccanico accoppiato, implementato nel codice di calcolo agli elementi finiti LAGAMINE. L'obiettivo era quello di calibrare un modello costitutivo sui dati osservati: il Barcelona Basic Model, con parametri appropriati, è in grado di rappresentare in modo soddisfacente il comportamento osservato.

Chapter 1

Introduction

1.1 Work objective

Purpose of this work is to characterise a specific bentonite-based material as regards its hydro-mechanical aspects, and to propose a suitable model describing its behaviour.
This study arises from a partnership between the University of Liege (Belgium) and the Politecnico of Milano (Italy), within a project of the latter one, which allows students to make a placement abroad under the supervision of both Italian and foreign researchers. In particular, this work takes part in a wider ongoing research project of the Geotechnology, Hydrogeology and Geophysics (GEO^3) Department of the University of Liege, focused on the underground waste disposal.
Most of the experimental tests have been performed in the geomechanical laboratory of Liege from November 2015 to February 2016, whereas the final editing work has been made at Politecnico.

1.2 Geological disposal for nuclear waste

Nuclear waste disposal is an actual issue in current society, since more than 400 nuclear reactors for electricity generation are operative nowadays, and more than 60 new nuclear plants are under construction worldwide (NEI, 2016). Together with the abandoned reactors and the radioisotopes used in other sectors such as industry, medicine, agriculture and research, they produce radioactive waste. This is defined as any substance that contains or is contaminated with radiotoxic nuclides in concentrations higher than those established by the competent authorities, and for which no subsequent use is foreseen, thus it must be disposed of (Villar, 2004).
Nuclear waste is generally classified depending on its radioactivity level:

low level waste (LLW), including waste generated from hospitals;

intermediate level waste (ILW), such as the nuclear reactor products emitted during their activity periods and during their decommissioning too;

high level waste (HLW), such as uranium and plutonium-239. It is characterised by high specific short-lived emitter activities and appreciable concentrations of long-lived alpha-emitting radiotoxic nuclides; moreover, it generates high temperatures (Villar, 2004).

The main concerns relative to the nuclear waste are its toxicity and its half-lives reaching up to many millions of years (Schaffer, 2011). Thus, long-term solutions have to be considered, in order to protect people and the environment: several countries, such as China, Belgium, France, Germany, Japan and Sweden, consider geological disposal as the best option, in order to physically and thermically isolate the nuclear waste within a deep storage, during its radioactive period (Skarlatidou, 2012; Wang, 2012).

1.2.1 Multi-barrier structure

High level nuclear waste is generally disposed of within stable geological formation at the depth of 500-1000 m (Goguel, 1987). In order to guarantee its thermal, chemical and physical isolation, a multi-barrier system (*Figure 1.1*) is implemented: several barriers, both natural and artificial, aim to prevent the possible escape paths for the radiotoxic nuclides to the surrounding environment (Villar, 2004).

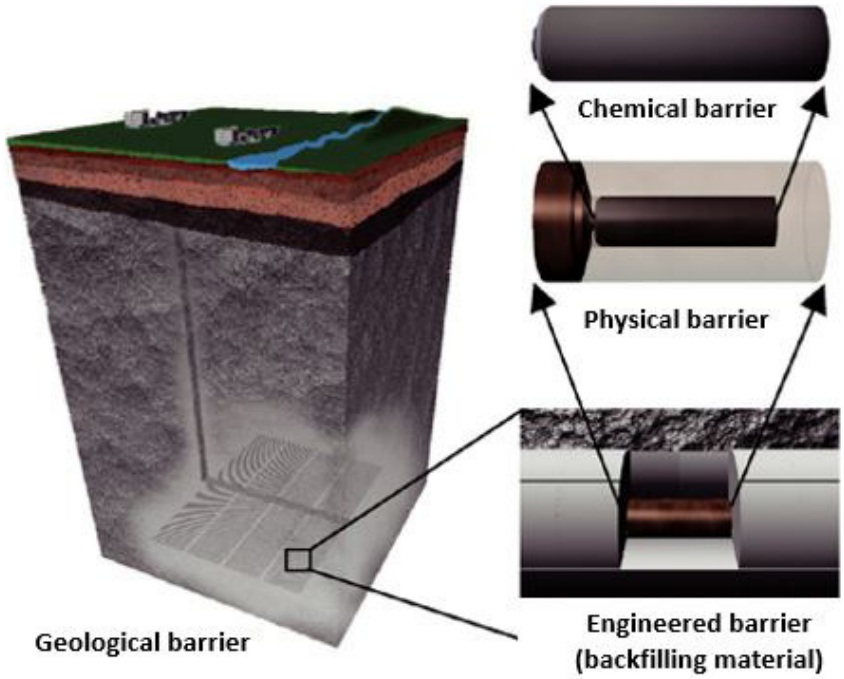

Figure 1.1: *Schematic representation of the multi-barrier system in a geological disposal facility (picture modified from JAEA, 2007)*

First of all, the radioactive waste is vitrified and immobilised in a solid, long-lasting and chemically inert matrix; it constitutes the first case: a **chemical barrier**.

Then, a high corrosion resistance canister confines and immobilises the waste: this is the **physical barrier**.

The canisters are placed in a series of chambers, shafts and drifts constituting the **engineered barrier**. The radius of these excavations has to be greater than the one of the canister, in order to host the **backfill material**: this one, on which behaviour this study is focused, acts as a sealing material, plugging the remaining space between the canisters and the chambers walls and between the canisters and the access shafts.

Finally, the geological formation hosts the whole installation, acting as a more external **geological barrier**.

1.2.2 Backfill material

The backfilling material exerts three basic functions in the context of geological disposals: from a hydraulic point of view, it has to contribute to the radiotoxic nuclide retention, by preventing the incoming and outgoing water flows, since the main nuclides transfer mechanism is the groundwater circulation. Moreover, the sealing material has a thermal function by contributing to heat dissipation (given the high heat quantity emanated by the high level waste), and a mechanical function by providing mechanical protection to the inner canisters (Villar, 2004).
Thanks to its properties, the most used sealing material in nuclear disposal application is saturated bentonite clay compacted at high density: the bentonite is an expansive clay and under these conditions it provides a very efficient isolation for preventing radiotoxic nuclides from reaching the surrounding biosphere. The most relevant characteristic of saturated compacted bentonite is its permanent swelling trend: thanks to it, by taking up water from the host rock and by swelling, it provides a self-sealing impervious barrier. Bentonite extruded by swelling can also seal the open rock joints surrounding the chamber, which would represent a preferential path for the nuclides leak (Pusch, 1979).
When the bentonite buffer is placed in the gallery, it gets hydrated and initially exhibits a swelling potential under free conditions, because of the unavoidable technological gaps between the geological environment and the contour of the engineered barrier. Under these unconfined conditions, the compacted swelling bentonite progressively fills both its pores and the technological gaps: the buffer density increases. Then, when the perfect contact between the buffer and the excavated surface is reached and the internal pores are filled, it swells under confined conditions, the backfill volume and thus the density are constant, and a swelling pressure starts to develop against the rock wall (Gatabin, 2016).
Hydraulic, mechanical, thermal and chemical properties of the compacted bentonite make it the most preferred sealing material in this kind of engineered applications. They are listed below (Villar, 2004).

As regards its *hydraulic* properties, it is characterised by a very low permeability, to reduce the percolation of groundwater.

From a *thermal* point of view, it has a sufficient thermal conductivity, to avoid excessive thermal gradients.

As regards its *mechanical* characteristics, it presents:

- mechanical resistance to the weight of the canister;
- suitable deformability, to ensure the absorption of the pressures generated by the host rock and by the hydration of the expansive component of the barrier;
- plastic behaviour to prevent the formation of fissures and to guarantee the homogeneous nature of the barrier;
- swelling potential to favour the self-sealing and the material homogeneity;
- non-excessive swelling pressure, to avoid damage to the system;
- low shrinkage in response to the drying occurring in the area surrounding the canister, due to high temperature; this represents an obstacle to the creation of a network of fissures;
- high plasticity index, meaning a large plastic range of the bentonite and ensuring ease in manufacturing, handling and transport.

From a *chemical* point of view, compacted bentonite has:

- high exchange capacity, meaning a high capacity in adsorbing ions in the event of radiotoxic nuclide leak;
- chemical stability, ensuring the longevity of the system (fundamental requirement given the long half-lives of the enclosed radioactive waste).

Some mixtures of expansive clay and aggregates such as crushed granite, quartz or graphite have been proposed by some agencies charged with the nuclear waste disposal, in order to increase the thermal conductivity of the barrier, improve its mechanical resistance and reduce the cost of the material.
Also different installation methods have been proposed: the most studied are pre-compacted bentonite blocks, but also the use of high density bentonite pellets combined with powdered bentonite has been investigated; this last method is easier to handle and install (Villar, 2004).

1.2.3 Expansive agents: smectites

Bentonite is defined as a rock «composed of a crystalline claylike mineral formed by the devitrification and the accompanying chemical alteration of a glassy igneous material, usually a tuff or volcanic ash» (Ross, 1945). Nowadays, the term bentonite has extended to any clay rock mostly constituted by minerals belonging to the smectite group; other minerals (quartz, feldspar, micas, etc.) are present in variable proportions.
Smectites are the responsible of the bentonite swelling capacity, since they have extraordinary expansive properties due to their chemical structure: they belong to the philosilicates group and are characterised by a T-O-T structural unit (*Figure 1.2*). This means that they are constituted by two tetrahedral (T) layers sandwiching a central octahedral (O) layer; because of it, they are also known

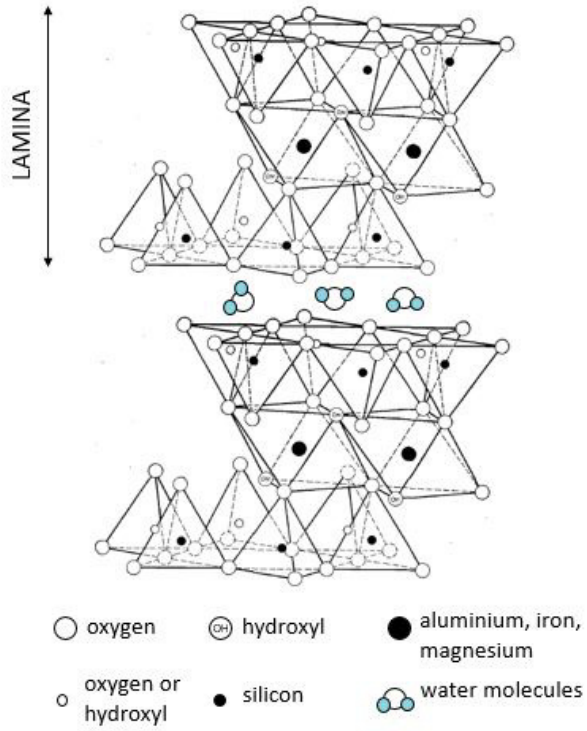

Figure 1.2: *Schematic representation of the structure of montmorillonite, the most common smectite (picture modified from Grim, 1953)*

as 2:1 silicates. T-O-T structures are defined as **laminae** and they indefinitely extend in longitudinal and lateral directions, whereas they are vertically piled up.
Oxygens or hydroxiles compose the tetrahedra and the octahedra vertices, and they surround an atom of silicon in the first case, and an atom of aluminium, iron or magnesium in the other case. All the vertices of the tetrahedra are arranged in such a way that they point towards the centre of the unit, and their bases constitute the external planes; moreover, the vertices of the tetrahedra lay on the same plane of the surfaces of the octahedra: the atoms common to the tetrahedral and octahedral layers are oxygens.
Because of their vertical piling-up, the lower and the upper oxygen layers of different layers are in contact; thus, laminae are negatively charged. For this reason, the positions between adjacent oxygen layers are usually occupied by exchange cations. This basically explains the swelling capacity of hydrated bentonite: in fact, water may enter between the two layers for solvation of the cations, causing the crystalline network to vertically expand. The lamina dimension depends on the hydration state and mostly on the kind of cations: when no molecules are located between the layers, each lamina is 9-10 Å high; after cations hydrations, this could increase to 16 Å for a sodic bentonite (Grim, 1953). By isolating and measuring the laminae, a first hypothesis on the kind of cations can be made (*Section 2.1*).
The piling of clay laminae forms **primary particles** (or **stacks**). The number of clay laminae present in each stack depends on the type of exchangeable cations: it is greater for bivalent cations (Ca or Mg) than for monovalent cations (Na).
A group of organised primary particles constitutes an **aggregate**.

The smectite organisation in laminae, stacks and aggregates seen before gives rise to three different kinds of porosity, which govern incoming water flow having different properties; the water in the different porosities is generally referred to as hydration water. The differences in porosity and the related water properties are listed below:

interlaminar or interfoliar porosity, with a dimension of the order of Å. Only polar molecules have access to it. The incoming water is the cation solvation water, influenced by the electrical field generated by the negative charge of the oxygen layers: it is a strongly bound internal water. Stepkowska (1990) proposed that this water may move freely in longitudinal and lateral directions, but not vertically;

intra-aggregate or microporosity, between adjacent primary particles. It includes pores having diameters smaller than 20 Å, although in high saturation states they may reach 35 Å. In these pores, the electrical potential decreases depending on the distance from the particles: at low distances, the water is adsorbed and cannot be separated from the clay particle; it is an internal water (Villar, 2004);

inter-aggregate porosity, classified as mesoporosity, if the pores have dimensions ranging between 0.002 μm and 0.05 μm, and as macroporosity if they are greater than 0.05 μm. The incoming water is retained by capillary or gravitational forces, and is defined as external water.

The bentonite swelling capacity depends on the adsorbed and flowing water in the smectite structure; this in turn depends on several factors, such as clay density, salinity of the pore water and type of exchangeable cation in the interlayer. It also depends on the water content, responsible for different chemical and hydraulic mechanisms: for low water contents, the adsorption is the predominant mechanism, it depends on the specific surface of the stacks and takes place in micropores; for high water contents, the capillary condensation is the main water driving force, it depends on the shape and the arrangement of the particles and takes place in the mesopores and macropores (Everett, 1973).

1.3 Work structure

An aim of the present study is to characterise a specific bentonite, suitable for nuclear waste disposal applications, in order to compare it with the already known types analysed in the literature. Different experimental tests will be performed to study its mineralogical composition, pore and particle size, plastic behaviour and hydraulic characteristics when it is compacted at high density.
Moreover, a swelling test will be performed in order to investigate the volume changes. This test allows to reproduce the hydro-mechanical behaviour of the compacted bentonite during its engineered application in nuclear waste disposal. A relation between the dry density and the exerted swelling pressure is expected, as highlighted in the literature.
Finally, different soil constitutive models, accounting for the coupled hydro-mechanical behaviour, will be calibrated and compared, on the basis of the obtained experimentally results.

Chapter 2

Soil characterisation

In order to perform an accurate characterisation of the used bentonite, some experiments are needed.
First of all, an X-Ray Diffraction will be performed in order to dive an estimation of the mineralogical composition of the studied bentonite.
Then, some experimental tests investigating the particle density will be needed: the particle density is an essential parameter, necessary in the most of the further tests. As shown below, this is a very difficult parameter to estimate: to solve some inconveniences, default hitches in an experimental work, a medium value from literature data will be considered and used in the current study.
Other important tests, with the purpose of analyse the macrostructure and the microstructure of the compacted soils, are the Granulometruic analysis and the Mercury Intrusion Porosimetry (respectively investigating on the particle and the pore size).
Finally, the Atterberg limits will be determined in order to better classify the soil and to analyse the range in which it behaves plastically.
After characterising the studied bentonite, a comparison with the known bentonite types will be made, to establish if the obtained values are physically reasonable and to eventually find some similarity with the known ones, useful also for establish the reliability of the results of the further hydraulic and mechanical tests.

2.1 X-Ray Diffraction

First of all, a diffraction test has been performed, with the purpose of investigating the mineralogical characterisation of the studied bentonite: this test is founded on the knowledge of how atoms are arranged into crystal structures and it allows to understand the synthesis, structure and properties of materials and, basically, which elements constitute them. In particular, an **X-Ray Diffraction (XRD)** analysis has been made: the diffraction method requires incident wavelengths comparable to the spacing between atoms, and x-rays match this preliminary condition, as their wavelength varies between 0.1 and 45 Å (Hatert, 2013).

2.1.1 Materials and methods

In order to perform the previously mentioned analysis, an x-ray diffractometer is needed; it consists of:

a source of x-rays, in particular a copper sealed x-ray tube;

a goniometer providing accurate mechanical movements of the sample and the detector, with respect to the copper tube;

an x-ray detector, generating a pulse of current every time it absorbs an x-ray;

electronics for counting detector pulses, according to the position of the goniometer.

The XRD analysis is physically founded on the *Bragg's law* (2.1), which can be derived from *Figure 2.1.* Chosen an angle of incidence θ for the incoming ray, and by looking at the two triangles ABC and ACD, it is possible to observe that they are similar, and so the angle in the ABC triangle is equal to θ. The interlaminar spacing d defines the difference in path length for the two rays, scattered respectively from the top lamina and from the bottom one; constructive wave interference occurs when the difference in path length for the two rays is equal to one wavelength λ or an integer multiple of it.

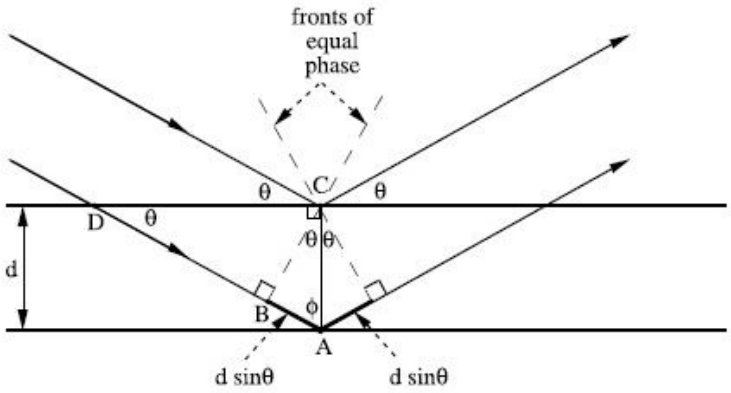

Figure 2.1: *Geometry for interference of a wave diffracted from two laminae separated by a distance* ***d****, (picture from Fultz, 2013)*

$$2dsin\theta = n\lambda \tag{2.1}$$

The method procedure consists of an incident wave direct into the target material and a detector moving about to record directions and intensities of the outgoing diffracted waves. A *θ-2θ diffractometer* has been used: the x-ray tube is kept stationary and the sample is rotated by an angle θ; to ensure that the scattered x-rays leave the sample at an angle θ, the detector must be rotated precisely by the angle 2θ. This kind of diffractometer is less versatile than a θ-θ one, which however requires more precise movement of the x-ray tube (Fultz, 2013).
Now, the crystal structure of the target material is determined thanks to a known geometrical relationship between the directions of waves interfering constructively and the crystal structure itself. The test allows to draw a spectrum of real space periodicities in a material, correlating the counts per second to the interlaminar spacing d (known thanks to the *Equation 2.1*); in fact, the wavelength λ only depends on the source material and it is equal to 1.54060 Å in this case. Starting from this spectrum, it is possible to deduce more information about the material, such as the constitutive elements and their percentage.

2.1.2 Experimental results

The *Figure 2.2* shows the experimental XRD spectrum for a sample of the studied bentonite. Each element has a characteristic interlaminar spacing d: starting from this, the corresponding element for each peak has been determined. Then, a semiquantitative analysis on the experimental spectrum allows to estimate the mineralogical composition of the studied bentonite: by producing with a dedicated software a theoretical spectrum with known elements but random percentages, it is possible to adjust the percentages in order to have the best of the matches between the theoretical spectrum and the experimental one. The elements and the relative percentages deduced in this way are listed in the *Table 2.1*.

Table 2.1: *Mineralogical composition of the studied bentonite*

Element	%
Montmorillonite	80
Quartz	11
Kaolinite	4
Cristobalite	3
Calcite	2

The clay minerals are represented by the montmorillonite and the kaolinite, which together compose the 84% of the studied materials: the first one belongs to the smectite group and it is responsible for the bentonite swelling behaviour; it is a T-O-T clay (or 2:1), meaning that it has two tetrahedral sheets of silica sandwiching a central octahedral sheet of alumina; kaolinite belongs to the kaolin group and it has only one octahedral sheet and one tetrahedral sheet (O-T or 1:1 structure) (Varma, 2002).

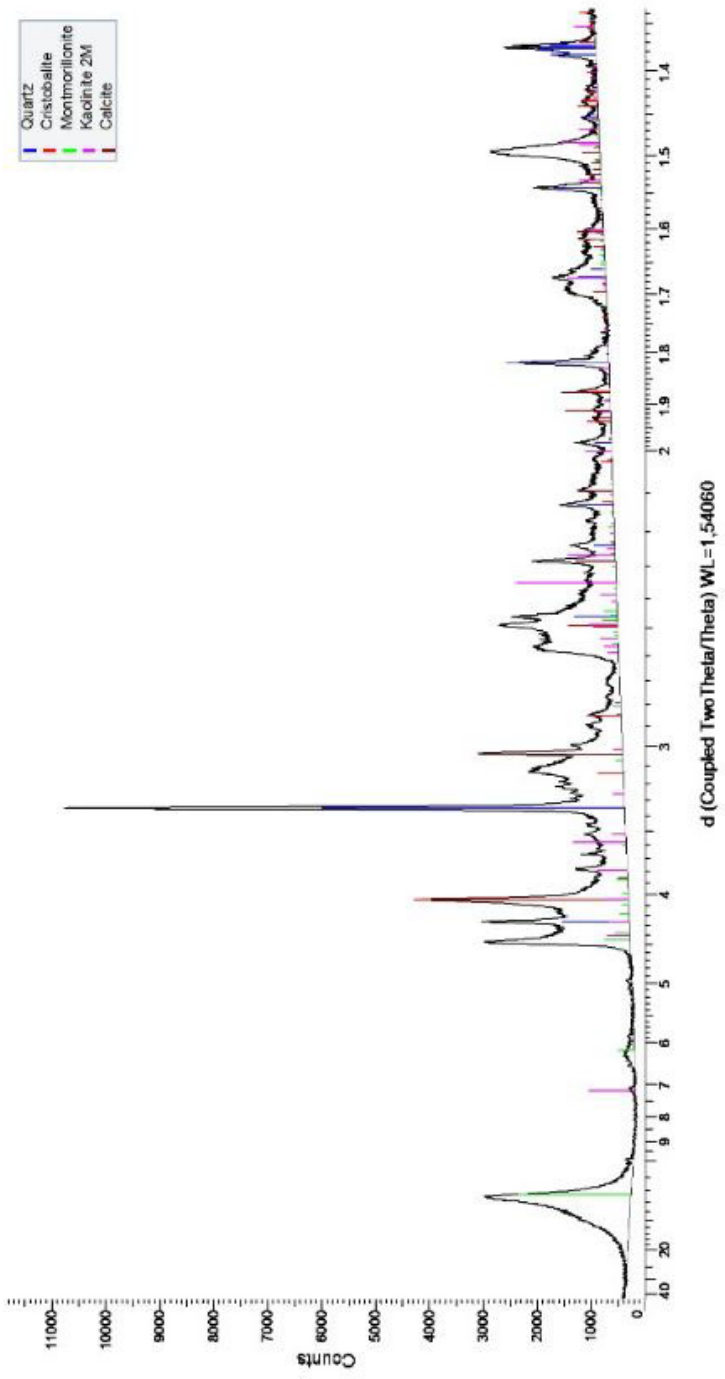

Figure 2.2: *Experimental XRD spectrum of the studied bentonite*

The quartz and the cristobalite are both silicon dioxide SiO_2 (14%): the cristobalite is a high-temperature polymorph of the quartz; it is an uncommon mineral, metastable at low temperatures. The calcite is a very common carbonate mineral with the chemical formula $CaCO_3$ (2%).
After the extraction of the clay fraction ($< 2\mu$m) and its drying out, to let the laminae settle, three different XRD tests have been performed in order to investigate the response of the bentonite clay fraction to different stirrings: *Figure 2.3* shows that in case of drying up to 550°C the interlaminar distance d is equal to 10 Å (red line), whereas it is equal to 12.5 Å in case of air drying at 20°(black line); finally, the analysed clay fraction has been saturated with ethylene glycol and the spectrum shows that the interlaminar distance d increases up to 18 Å (blue line). The aim of this test is to detect the swelling in a microstructural scale, by observing an increasing interlaminar distance with an increasing hydration. An interlaminar distance d equal to 12.5 Å could explain the presence of a sodium bentonite: in fact, a monovalent cations bentonite (e.g. Na) has only one water layer between the laminae, whereas a bivalent cations one (e.g. Ca or Mg) has two water layers, meaning an interplanar distance ranging between 14 and 15 Å. Since the black peak, corresponding to an air drying of the clay fraction, is not perfectly symmetrical, this could even signify the presence of both monovalent and bivalent cations. Further experiments would be needed to certainly affirm it.

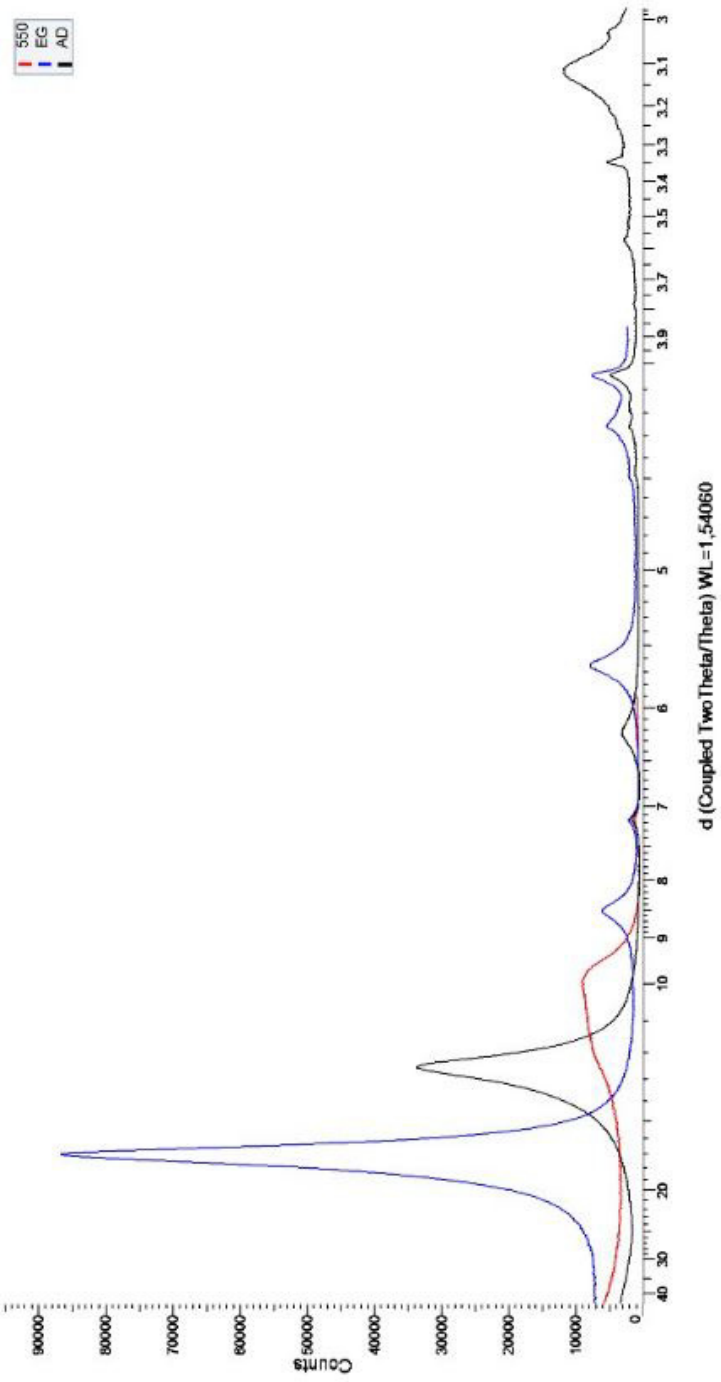

Figure 2.3: *Experimental XRD spectrum of the clay fraction of the bentonite sample, in order to detect the swelling trend of the smectites with increasing hydration*

2.2 Particle density ρ_s determination

The **particle density (or true density)** $\boldsymbol{\rho_s}$ is an important parameter of soils, as many other tests explained in the following paragraphs (such as the mercury intrusion porosimetry, the granulometric analysis and the determination of the swelling pressure) are performed starting from it. That is the reason why two different tests have been made, with the purpose of determining the value of the particle density; unfortunately, both the experiments gave non-suitable results and an average value from literature was assumed.
The particle density ρ_s is defined as the ratio between the mass of the soil particles M_s and the volume of the solid fraction V_s, without considering the empty space:

$$\rho_s = \frac{M_s}{V_s}. \tag{2.2}$$

Whereas the mass is easily measurable by way of a scale, the problem arises for the determination of the solid volume: in fact, the two different used methods provide the estimation of the solid volume; in particular, the bentonite solid volume is very difficult to estimate for different reasons, analysed below. After assessing it, the particle density ρ_s is calculated through the *Equation 2.2*.

2.2.1 Water pycnometer

Materials and methods

Water pycnometer provides the determination of the particle density of soil solids passing the 4.75 mm sieve.

Materials The needed apparatus for this test method consists of:

water pycnometer, i.e. a stoppered flask with a minimum capacity of 250 ml (*Figure 2.4*);

precision scale (0.01 g);

thermostatically controlled drying oven capable of maintaining temperatures of 110±5°C, for drying moist samples;

vacuum pump;

non-corrosive smooth surface funnel with a diameter of the stem large enough to let the soil solids pass through;

distilled water;

mortar and pestle.

Methods A mass of oven-dried specimen is considered: all clusters of soil are broken up with the pestle within the mortar.
The sample is placed in the pycnometer through the funnel and the mass M_{ps} is measured. Distilled water is added until the level is between 1/3 and 1/2 of the depth of the main body of the pycnometer: a slurry is formed by agitating the water. The vacuum pump allows to remove the entrapped air in the soil

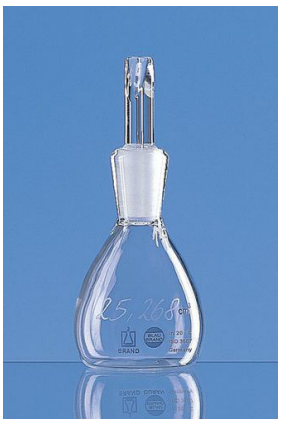

Figure 2.4: *Water pycnometer (picture from 3R, 2016)*

slurry: the pycnometer must be continually agitated under vacuum for at least 2 hours, in order to make the clay soil solids remain in suspension and the slurry in constant motion; bubbles form at the beginning of the deairing process.
The pycnometer is filled with distilled water up to a calibration mark: the mass of the pycnometer filled with only distilled water up to that mark has been previously weighted during the calibration phase (M_{pw}). The mass of pycnometer, soil and water (M_{pws}) is measured and recorded.
The principle on which the *water pycnometer test* is based is described below:

as the volume of the solid soil V_s is impossible to be directly determined, the calculations are made starting from an equal volume, occupied by a certain water mass M_w, where ρ_w is the water density, assumed constant and equal to 1'000 kg/m^3;

$$V_s = \frac{M_s}{\rho_s} = \frac{M_w}{\rho_w} \tag{2.3}$$

the water mass M_w is determined from the difference of the mass of the pycnometer filled with only water (M_{pw}) and the mass of the pycnometer filled with water and soil except for the soil mass (M_{pws}-M_s),

$$M_w = (M_{pw} - (M_{pws} - M_s)); \tag{2.4}$$

the mass of dry soil (M_s) is determined by the difference between the mass of the pycnometer including the sample (M_{ps}) and the known mass of the empty pycnometer (M_p)

$$M_s = (M_{ps} - M_p); \tag{2.5}$$

therefore, the particle size ρ_s is calculated by

$$\rho_s = \frac{M_s}{V_s} = \frac{M_s}{\frac{M_w}{\rho_w}} = \frac{M_s}{\frac{M_{pw} - (M_{pws} - M_s)}{\rho_w}} \tag{2.6}$$

Table 2.2: *Experimental results obtained by the water pycnometer test*

	Measured	**Calculated**
M_p	121.275 g	
M_{ps}	123.692 g	
M_s		2.417 g
M_{pw}	220.033 g	
M_{pws}	221.675 g	
V_s	0.775 cm^3	
$\boldsymbol{\rho_s}$		**3'119 kg/m^3**

Experimental results

Table 2.2 shows the results obtained during the experimental test. The obtained results are much higher than the common value of particle density for bentonite: that means an underestimation of the solid volume V_s. On the contrary, the opposite behaviour was expected: in fact, the bentonite sample could swell in contact with distilled water and so the measured volume could be overestimated. This is the reason why the water pycnometer method is usually discarded in case of swelling materials.

2.2.2 Gas expansion pycnometer

Materials and methods

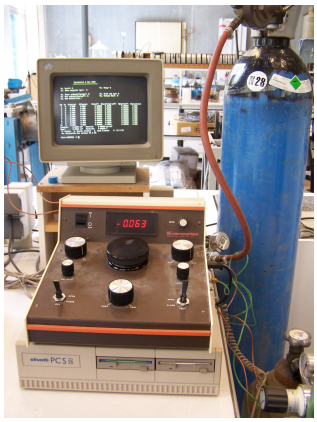

Figure 2.5: *MultiVolume Pycnometer 1305 (picture by Sara Rozzoni)*

The gas expansion pycnometer (*Figure 2.5*) has to be preferred to the traditional one in case of swelling material. Gas is preferable because, due to its small atomic dimension, it can occupy even the smallest voids of the sample, in order to obtain its real volume: the best choice is to perform this experiment with helium. In fact, this is the element with the minimum atomic radius; moreover, it has a high thermal conductivity which means, in thermally controlled experiments, precise and fast results. Nevertheless, considering the laboratory

availability and the satisfying performance of nitrogen, this has been employed in the pycnometer test.
The gas expansion pycnometer is a laboratory device based on the principle of the gas movement, suitable for precisely determining the real volume of powders, with a guaranteed accuracy of the measurements of 0.1%.
It consists of two chambers divided by a valve; the chambers volume is known from a previous calibration. The first chamber containing a known mass of the sample is pressurized with nitrogen up to a pressure p_1; the second one is empty. Then, the valve is opened and the subsequent expansion of the gas into a second precisely measured volume, known as expansion chamber, results in a pressure drop. Now, the sample is submitted to a pressure p_2, smaller than p_1.
A simplified operating schema of the gas expansion pycnometer is represented in *Figure 2.6.*

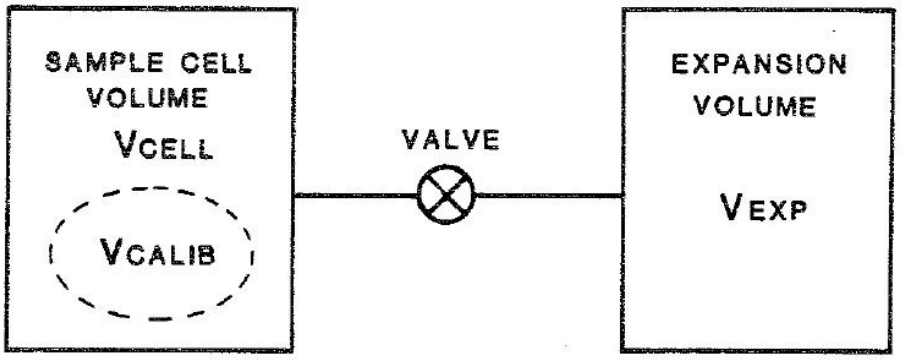

Figure 2.6: *Simplified operating schema of the gas expansion pycnometer (Micrometrics, 1986)*

As the temperature can be considered constant during the whole experiment duration, the volume of the soil particle V_s has been calculated starting from the *Boyle-Mariotte law* (2.7): by comparing the two moments, before and after the valve opening, the product of the pressure multiplied by the volume occupied by the nitrogen is constant. At first, the nitrogen occupies the whole volume of the first chamber V_{cell} except for the volume of the sample V_s; then, it occupies both the first chamber V_{cell} and the expansion chamber V_{exp} except for the volume of the sample.

$$p_i V_i = constant \tag{2.7}$$

$$p_1 \cdot (V_{cell} - V_s) = p_2 \cdot (V_{cell} + V_{exp} - Vs) \tag{2.8}$$

$$V_s = V_{cell} - \frac{V_{exp}}{\frac{p_1}{p_2} - 1} \tag{2.9}$$

Experimental results

Table 2.3 shows the measured data.

By applying the *Equation 2.9* for the different measurements and by averaging the results, the particle density ρ_s of the studied bentonite is equal to

Table 2.3: *Measured data*

$\mathbf{M_s}$ (g)	P1 (kPa)	P2 (kPa)	$\mathbf{V_{cell}}$ ($\mathbf{m^3}$)	$\mathbf{V_{exp}}$ ($\mathbf{m^3}$)
0.127	134.71	77.74	$8.69 \cdot 10^{-6}$	$6.33 \cdot 10^{-6}$
0.127	134.58	77.67	$8.69 \cdot 10^{-6}$	$6.33 \cdot 10^{-6}$
0.127	134.10	77.39	$8.69 \cdot 10^{-6}$	$6.33 \cdot 10^{-6}$
0.127	133.96	77.31	$8.69 \cdot 10^{-6}$	$6.33 \cdot 10^{-6}$

2'364 kg/m^3: this value cannot be accepted because it is much lower than the common value of particle density for bentonite-based soils.
In this specific case, the gas expansion pycnometer method has overestimated the solid volume V_s: the imposed pressure has caused the compaction of the sample, making it difficult to nitrogen atoms to penetrate in each empty space. In order to solve this inconvenience, one may suggest to use lower pressure P1, but this could not assure the total penetration of the nitrogen into the pores, overestimating the solid volume one more time.

2.2.3 Discussion

Romero (2013) proposes a constant value for the bentonite particle density, equal to 2.65 Mg/m^3; a posteriori analysis on the studied bentonite characterisation will give a great similarity with the MX-80 bentonite (see *Section 2.6*), which has a particle density of 2.82 Mg/m^3. Since both the performed experimental tests have given non-acceptable results, an average value of 2.74 Mg/m^3 has been assumed.

2.3 Granulometric analysis

As soils are aggregates of different particles sizes, a granulometric analysis is needed to describe the frequency distribution of the grain sizes and their variation field. The aim is to trace a curve relating the particle size to the passing percentage in weight of finer grains: the grain size distribution curve.
Depending on the soil type, two different methods can be used: a **sedimentation analysis** for the fine-grained soils and a **sieve analysis** (also called gradation test) for the coarse-grained ones.
In this study, both of them have been used: the first one for the smaller portion of the sample (according to the NF P94-057), and the second one for the coarser portion of it (diameters greater than 74 μm).

2.3.1 Materials and methods

2.3.2 Materials

In order to perform a granulometric analysis of the studied bentonite, the following materials have been used during the experimental tests:

precision scale (0.01 g)

deflocculant (sodium hexametaphosphate)

distilled water

burette

mixer

thermostatic bath

graduated aerometer

sieves with different opening sizes (2.380 mm, 1.190 mm, 590 μm, 297 μm, 149 μm, 74 μm)

mechanical sieve shaker

thermostatically controlled drying oven, capable of maintaining temperatures of 110±5°C, for drying moist samples.

2.3.3 Preparation of the sample

First of all, a sample of bentonite has been put in the oven for 24 hours, in order to determine its water content w. This is important, in order to calculate the dry mass M_s of the bentonite employed in the granulometric analysis, starting from the wet mass M.

$$w = \frac{M - M_s}{M_s} \tag{2.10}$$

Then, 500 ml of distilled water and 125 ml of deflocculant have been added to the chosen bentonite mass (M=34.32 g). After 24 hours of rest, the solution has been mixed for 1 minute and distilled water has been added in order to have a total volume equal to 1 l (Peltier, 1969).

2.3.4 Methods

Sedimentation analysis The burette containing the suspension has been placed in the thermostatic bath, up to an equilibrium temperature of 20 °C. Once reached, the burette has been manually agitated for 1 minute and then replaced in the thermostatic bath.
Measurements have been taken on the graduated aerometer at various time intervals up to 24 hours, as shown in *Table 2.4*. The aerometer is an instrument measuring the liquid densities: the more the material sediments, the more its density decreases and the Archimedes' buoyant force too; this produces a sinking of the aerometer which can be directly related to the suspension density, through a previous aerometer calibration. The measurement Rt and the real density Rr are related by the following equation:

$$Rr = Rt + Kt + Km - Kd \tag{2.11}$$

where:

Kt is the temperature correction, equal to 0 for 20°C;

Km is the meniscus correction, i. e. the difference between lectures on the top and on the bottom of the meniscus, it is equal to 0.1 in distilled water;

Kd is the deflocculant correction, equal to 3.5 for 125 ml of sodium hexametaphosphate.

In order to trace a grain size distribution curve, it is fundamental to know the percentage of finer material for a given particle size; starting from the density of the suspension it is possible to calculate the percentage of material smaller than an equivalent diameter (2.12),

$$Finer(\%) = \frac{100}{M_s} \frac{\rho_s \rho_w}{\rho_s - \rho_w} (aRr - Lz) \tag{2.12}$$

where:

M_s is the dry mass, calculated with the *Equation 2.10*;

ρ_s is the particle density, assumed equal to 2'740 kg/m^3 according to what is discussed in 2.2;

ρ_w is the water density, equal to 1'000 kg/m^3;

a is a coefficient due to the aerometer calibration;

Lz is the zero-measurement when the burette contains only water.

For each measure time, the equivalent diameter is calculated through the *Stokes' law* (2.14), relating the particle size squared D^2 to the sedimentation velocity v:

$$v = \frac{Hr}{t} \tag{2.13}$$

$$v = \frac{\rho_s - \rho_w}{18\eta} g D^2 \tag{2.14}$$

where:

Hr is the path travelled by the particles during the time t; it is directly linked to the calculated density Rr through two constants obtained by the aerometer calibration;

η is the water dynamic viscosity, equal to 10^{-3} Ns/m^2 in case of water at 20°C;

g is the gravitational acceleration 9.81 m/s^2;

D is the equivalent diameter expressed in m.

The grain size distribution curve for the fine-grained part of the sample can be traced by correlating the equivalent diameter and the percentage of finer material at the same time.

Sieve analysis Then, the sample has been dried for 24 hours in the oven to perform the classic sieve analysis for the coarser portion. The sieves are nested in series in order of decreasing size of opening; after having placed the sample on the top sieve, the whole column is automatically agitated by the mechanical sieve shaker. After this, the portion of the sample retained by the i sieves is weighted, and the finer percentage is calculated by:

$$Finer(\%) = 100 - \frac{\Sigma_{j=1}^{i} W_{retained(j)}}{W} * 100 \tag{2.15}$$

The obtained value corresponds to the percentage of the sample smaller than a specific size, and these two measures represent one point on the grain size distribution plan. By calculating the passing percentage for each sieve, it is possible to obtain a curve for particles bigger than 74 μm: this is the sieve with the smallest size of opening available, according to the NF P94-057.

2.3.5 Experimental results

Tables 2.4 and *2.5* show the obtained values for both the sedimentation and the sieve analysis; for the latter one, the ASTM sieve (*American Society Standard Material*) number is specified.

Table 2.4: *Sedimentation analysis*

t (s)	**Rt (g/dm³)**	**Rr (g/dm³)**	**Hr (cm)**	**D (μm)**	**Passing (%)**	**Retained (%)**
60	41.50	40.04	10.04	42.21	96.38	3.62
120	41.00	39.54	10.13	29.97	94.94	5.06
300	39.80	38.34	10.33	19.15	91.48	8.52
900	38.50	37.04	10.56	11.17	87.73	12.27
2700	37.00	35.54	10.81	6.53	83.41	16.59
7200	35.80	34.34	11.02	4.04	79.95	20.05
18000	34.20	32.74	11.29	2.58	75.34	24.66
86400	31.20	29.74	11.81	1.21	66.69	33.31

Table 2.5: *Sieve analysis*

N.ASTM	D (μm)	Finer (%)	Retained (%)
50	297	99.88	0.12
100	149	99.45	0.55
200	74	97.26	2.74

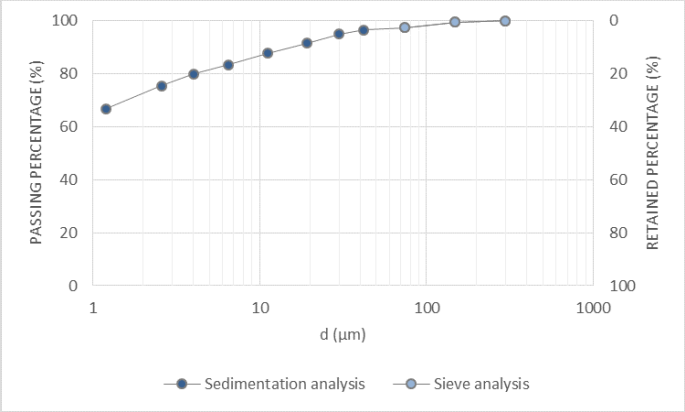

Figure 2.7: *Grain size distribution curve*

The **grain size distribution curve** built starting from them is shown in *Figure 2.7*.

From the curve, it is possible to deduce a clay percentage ($< 2\mu$m) equal to 73%. According to the MIT (*Massachussetts Institute of Technology*) classification system (Shroff, 2003) , the studied bentonite is made by about 73% of clay, 24% of silt (2μm<d< 60μm) and 3% of sand (60μm<d<2 mm).

Usually, a grain size distribution curve ranges from 0% to 100%: in this study, given the high percentage of small particles, the curve ranges between 60% and 100% only because of a time limitation; smaller percentages, corresponding to smaller densities, could have been measured by taking measurements after more than 24 hours.

2.4 Mercury Intrusion Porosimetry

In order to quantitatively detect the microporosity structure and the pore size distribution of the bentonite, a Mercury Intrusion Porosimetry test has been performed both on the powder and on the compacted bentonite. In the first case, the pore size depends only on the previous history of the material and on its fabrication process; in the second one, the aim is to identify a bimodal pore size distribution typical of compacted clays, as explained in *Chapter 1.*

2.4.1 Materials and methods

The needed equipment consists of:

a thermostatically controlled drying oven capable of maintaining temperatures of 110±5°C for drying moist samples;

a precision scale (0.01 g);

a porosimeter.

The latter one basically consists in a device applying a pressure on a mass of mercury, to make it penetrate inside the pores. It consists of a sample holder (called penetrometer), a pressure generator which produces the mercury intrusion, and some transducers to measure the intrusion volume and pressure. The porosimetry employs mercury because of its high surface tension γ and contact angle θ: it is a non-wetting fluid, which implies that it is not absorbed from the surface pores by capillary mechanism. The one used in this test is the *Triple-Distilled-Mercury.*
The intrusion process depends on the inlet accessibility of a pore, and it takes place from the external part of the sample to the inner one. The volume of mercury that penetrates the pores under a given pressure is measured by the device itself. This volume corresponds to the volume of pores of given radius (*Equation 2.16*). The Mercury Intrusion Porosimetry can investigate pores of sizes ranging between 500 μm and 3.5 nm. With the following limiting assumptions (*Figure 2.8*):

parallel, cylindrical and non cross-linked pore geometry;

inlet size representative of the effective pore size;

absence of closed pores, since the mercury cannot reach them;

the pore radius can be assessed by the Washburn equation (Giesche, 2006):

$$\Delta P = \frac{2\gamma cos\theta}{r_{pore}} \tag{2.16}$$

where:

ΔP is the pressure applied to the mercury to penetrate the pores;

γ is the surface tension of mercury, equal to 0.485 N/m;

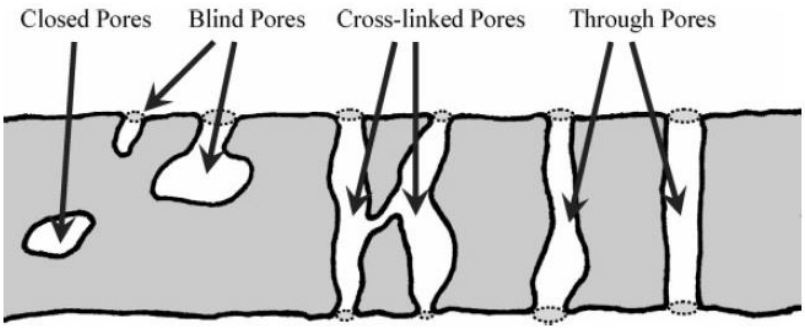

Figure 2.8: *Schematic representation of different kinds of pores (Giesche, 2006)*

θ is the contact angle between the solid and the mercury; the mercury is a non-wetting fluid and so its contact angle is bigger than 90°. It is usually equal to 130°or 140°: in the present study it has been considered equal to 130°;

r_{pore} is the pore size estimated under the above-cited hypothesis.

Thus, the pore radius r_{pore} can be determined as a function of the applied pressure, the surface tension and the contact angle of mercury.
Since any water content may damage the porosimeter, a dried or lyophilised sample is needed. In order to maintain the real structure of the material, the second option is preferable because it freezes the material through liquid nitrogen and allows to remove the contained frozen water by sublimation.
Unfortunately, due to the unavailable lyophilisation device, samples have been dried at the oven for 24 hours at a standard temperature of 105°.

2.4.2 Experimental results

Three tests have been performed on dried bentonite at different physical states and densities. Thus, the results are different and in particular they show decreasing macropore size with increasing dry density.

As regards the powder bentonite, the test detects a peak around 7/8 μm (*Figures 2.9*), exclusively due to the fabrication process. In this case, there is not a difference between macropores and micropores, but the peak indicates the size of the void spaces between the grains. The porosity reaches a value of 0.63 (*Figures 2.10*).
When the sample is compacted, it is usually possible to distinguish between macroporosity and microporosity: in this case the expected bimodal distribution is not very clear. However, it is possible to observe a double porosity in the less compacted sample (blue curve): the peak around 2 μm explains the relevant presence of macropores with this diameter, represented by a clear step in *Figure 2.9*; a less marked peak states the micropores, more uniformly distributed, around 0.01 and 0.2 μm.

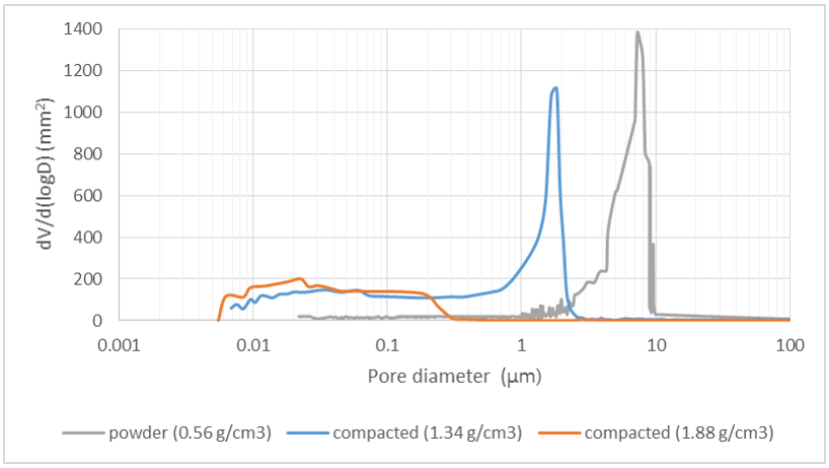

Figure 2.9: *Pore size distribution curves*

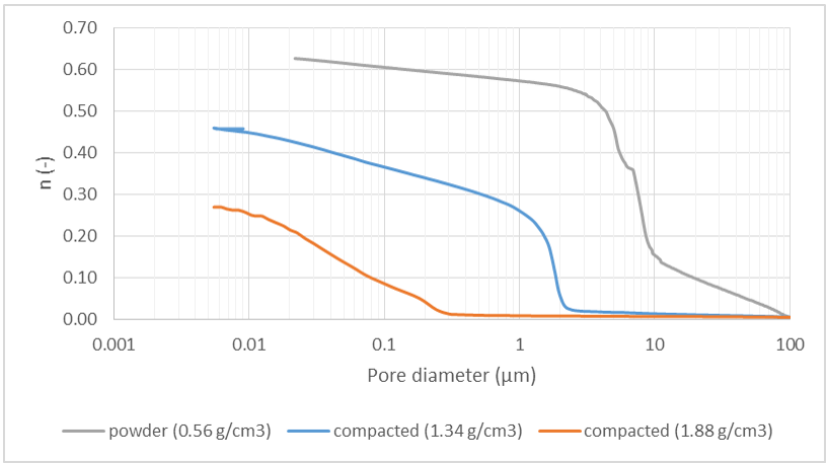

Figure 2.10: *Cumulative porosity curves*

An uniform pore distribution is also detectable from the more compacted sample (orange curve): in the above-cited size range, the two curves are quite well superimposed in *Figure 2.9* and they show the same slope change in *Figure 2.10*. On the other hand, it does not show any peak related to the macropores. This could be explained by the greater compaction level; in fact, the compaction affects the macropores reducing their size, and leaves the micropores undisturbed.
By comparing the obtained results with the literature data, a partial agreement with Saba et al. (2014) is inferable: a similar peak value for the smaller pores (0.02 μm) defines the characteristic size of the sample microstructure. On the other hand, a greater value (more than 10 μm) has been assessed for the macrostructure: that can be explained by the different grain sizes distribution curves. In fact, although the dry density is comparable with the ones used in this work, the percentage of sand, equal to 35%, is much larger than the one of the current study (3%). Since the macropore size is related to the coarse-grained fraction, this difference would explain the different size of macropores.

The Mercury Intrusion Porosimetry test has indicated a rather indisturbed intrinsic microstructure of the compacted bentonite, and a variable macrostructure depending on the compaction rate. The more the bentonite is compacted, the smaller the macropores volume is; and the more it is compacted, the more it swells, as shown in *Section 4.3*. Thus, a Mercury Intrusion Porosimetry test could indicate an optimum dry density value, for which the macropores are already closed; it means that the swelling and sealing process of the bentonite buffer would start before, producing faster and better performances.

2.5 Atterberg limits

Whereas the hydro-mechanical behaviour of the coarse-grained soils can be explained by the particles size, for the fine-grained soils it is the mineralogical composition that governs their physics. Then, in well defined conditions, the water content can explain the mineralogical composition of the soil (Lancellotta, 2012). The *Atterberg limits*, from the Swedish researcher who introduced them, are the water contents corresponding to the threshold between defined physical states: in fact, soil consistency can vary highly depending on the interstitial water contained in the pores and on the thickness of the adsorbed water layer covering the particles.
Three thresholds are defined between different physical states:

Table 2.6: *Atterberg limits related to the soil physical states*

Physical state	**Atterberg limit**
Solid state	
	Solid limit $\mathbf{w_S}$
Semi-solid state	
	Plastic limit $\mathbf{w_P}$
Plastic state	
	Liquid limit $\mathbf{w_L}$
Liquid state	

The solid limit w_S represents the threshold between the solid and the semi-solid state. It has not been calculated in this study because of the unavailability of necessary devices in the laboratory: however, it is not a significant parameter for the purpose of this work; more interesting are the liquid and the plastic limits, as they define the bentonite plastic range, that is the aptitude of the material to be modelled and deformed without breaking or fracturing.

2.5.1 Liquid limit $\mathbf{w_L}$

Materials

The **liquid limit $\mathbf{w_L}$** is the threshold between the liquid state and the plastic one, and it is experimentally defined as the water content at which the two halves of an analysed mass placed in a standardized cup rejoin themselves along a length of 10 mm and after 25 blows (Peltier, 1969).
The following devices are used to determine the liquid limit w_L:

distilled water;

a spatula to blend and arrange the soil;

a Casagrande cup - this is a device made up of a hard rubber base, a camshaft equipped with a crank and a spherical cap shaped cup linked to the crank and containing the soil mass (*Figure 2.11*);

a standardized grooving tool (*Figure 2.11*);

suitable resistant containers with close-fitting lids to avoid moisture exchanges - one container for each water content determination;

precision scale (0.01 g);

a thermostatically controlled drying oven capable of maintaining temperatures of 110±5°C for drying moist samples.

(a) *Casagrande cup (picture by Sara Rozzoni).*

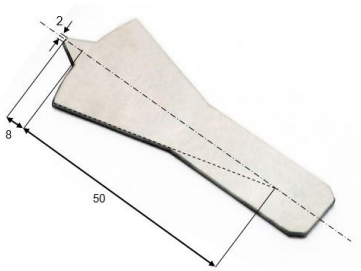

(b) *Standardized grooving tool (picture modified from Controls Group, 2015).*

Figure 2.11: *Casagrande cup for the determination of the liquid limit*

Method

100 g of bentonite are hydrated with distilled water, and blended in order to obtain an uniform play dough: in case of clay materials, the sample has to rest for 18 hours in a closed container, to allow the homegenization of water content. The obtained dough is placed in the Casagrande cup and adequately arranged with the help of the spatula: the surface is levelled to a maximum thickness of around 1 cm. A groove is made in the middle of the soil along the axial plane by a standardized tool: this has to be kept perpendicular to the cup surface and the groove has to be about 40 mm long (Peltier, 1969).
By rotating the crank, the cup is repeatedly dropped from 10 mm onto the hard rubber base at a rate of 2 blows per second, during which the groove gradually closes as a result of the impacts (Peltier, 1969). It is important to take note of the number of blows needed to make the two edges of the groove close up at the basis for a length at least equal to 10 mm.
The first sample has to be made with a dough slightly under its liquid limit: the number of blows has to be included between 15 and 22. If it is lower than 15 the dough can be hydrated and blended up to homogeneity; if it is greater than 22 the dough has to be dried by still resting or by blending it on the work surface area (Peltier, 1969).
After the first one, different samples and tests are made but only numbers of blows included in a range between 15 and 35 are considered. After each test, a sample of material, taken with the spatula from both the two edges of the groove and next to its closure, is put into a suitable container and immediately

weighted to avoid mass loss due to evaporation. The associated water content is calculated by the *Formula 2.10*, after leaving the sample in the oven for 24 hours.
Now, each couple of values *water content w - number of blows* represents a point in the same plane. By tracing the obtained points in a semi-logarithmic scale, the number of blows on the x-axis in logarithmic scale and the water content on the y-axis in arithmetic scale, they have to lay on a straight line. The liquid limit w_L is the water content corresponding to 25 blows on the regression line. If points are highly scattered and they do not lay on a line, the experiments have to be repeated.

Experimental results

Table 2.7 and *Figure 2.12* show the results obtained in the laboratory: the range for the liquid limit is usually very tight for bentonite-based soils; for this reason it is difficult from an experimental point of view to vary the water content and to remain between 15 and 35 blows. That is the reason why only three samples gave an acceptable number of blows, while the other ones were out of the admissible range: a minimum change in the water content, by drying or by wetting, can widely modify the bentonite characteristics and its response to mechanical actions.

Table 2.7: *Experimental data for the determination of the liquid limit*

M (g)	**M_s (g)**	**Water content w (-)**	**Nr. of blows (-)**
5.70	1.12	4.1012	16
6.27	1.23	4.0951	20
4.61	0.91	4.0861	25

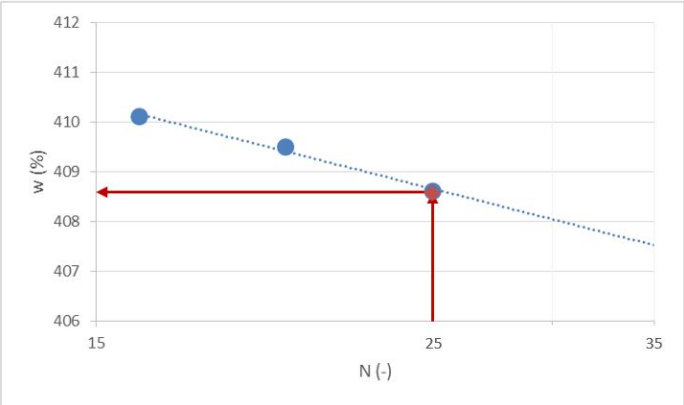

Figure 2.12: *Linear regression from the experimental data*

The liquid limit w_L estimated by following the described procedure is equal to **408.59%**.

2.5.2 Plastic limit w_P

Materials

The **plastic limit w_P** is the threshold between the plastic state and the semi-solid one, and it is experimentally defined as the water content at which a thread 100 mm long and 3.2 mm in diameter, rolled out on a flat non-porous work surface area, breaks apart in pieces 10-20 mm long (Peltier, 1969).
The needed equipment includes:

distilled water;

wood or plexiglass panel about 6x10 cm;

a marble work surface area;

some spatulas;

a calibrated bar with a diameter equal to 3.2 mm;

suitable resistant containers with close-fitting lids to avoid moisture exchanges - one container for each water content determination;

precision scale (0.01 g);

a thermostatically controlled drying oven capable of maintaining temperatures of 110±5°C for drying moist samples.

Method

The plastic limit w_P is usually determined after the liquid one: in this case, the sample is too much wet and it is made by blending it and by rolling it on the marble.
Starting from little balls of dough, different threads 100 mm long and 3.2 mm in diameter are rolled and modelled by hand on the wood or plexiglass panel, and compared to the calibrated bar. If the initial ball breaks apart before making the threads, it means that the soil has a water content lower than the plastic limit and some water has to be added. Otherwise, if the thread does not show any fissures, the soil water content is greater than the plastic limit and the dough has to be dried by blending and by rolling it on the marble: it is absolutely wrong to add dry powder to the wet mass in order to dry it, especially for clay-based materials, because they need a long time to get homogenized (Peltier, 1969).
The plastic limit is reached when a thread with a diameter of 3.2 mm breaks apart in pieces 10-20 mm long: these pieces are placed in suitable containers, weighted, dried in the oven for 24 hours and re-weighted. The water content is calculated with the *Formula 2.10* and the plastic limit is calculated as the arithmetic mean of different samples (Peltier, 1969).

Experimental results

Table 2.8 shows the experimental results for two different samples.

Samples are considered acceptable when the standard deviation is lower than the 2% of the average water content; otherwise an additional test has to be performed (Peltier, 1969): the two tests reported have a standard deviation

Table 2.8: *Experimental data for the determination of the plastic limit*

M (g)	**M_s (g)**	**Water content w (-)**
1.64	1.05	0.5694
1.85	1.17	0.5773

equal to 0.4%.
The plastic limit w_P estimated by following the described procedure is equal to **57.33%**.

2.5.3 *Unified Soil Classification System* plasticity chart

A granulometric-based soil classification is not representative of the hydro-mechanical behaviour of fine-grained materials such as clays and silts. It depends instead on the kind of constitutive minerals; in order to characterize the studied bentonite and to permit a comparison with other bentonite soils known from the literature, some indexes directly derived from Atterberg limits and clay percentage are listed below.

Plasticity is one of the most important properties of fine-grained soils, defined as soils having the percentage of finer at the ASTM 200 greater than 50%; therefore, this is the first parameter of classification: the most plastic soils are defined as clays, while the less plastic or non-plastic fine-grained soils are named silts. A way to represent the size of the range of water contents where the soil exhibits plastic properties is the **plasticity index PI**:

$$PI = w_L - w_P \tag{2.17}$$

The second most important index property in fine-grained soils classification is the limit liquid w_L: soils with a liquid limit equal or greater than 50% have a high liquid limit (H); otherwise they have a low liquid limit (L).

The *Unified Soil Classification System* (USCS) plasticity chart takes into account both the plastic index and the liquid limit, in order to classify the fine-grained materials.
The USCS, developed by Casagrande in 1948, is the most common classification system used in the civil engineering; it is adopted by the *Bureau of Reclamation* and by the *US Army Corps of Engineering of the United States*, and suggested by the AGI (*Associazione Geotecnica Italiana*) recommendations (Lancellotta, 2012). According to this system, soils are divided in five main groups: gravels and sands as the coarse-grained materials, inorganic silts, inorganic clays and organic soils as the fine-grained materials. Whereas the classification for gravels and sands is basically grounded on a granulometric analysis, for the fine-grained soils it depends on the liquid limit w_L and on the plastic index PI.
The plasticity chart is a graphic representation: it is constructed with the liquid limit w_L as abscissa and the plastic index PI as ordinate; both axes are

expressed in percentage. Three straight lines divide the plane into five suitable areas:

$$w_L = 50 \tag{2.18}$$

dividing high liquid limit soils (H) from low liquid limit ones (L);

$$PI = 0.73(w_L - 20) \tag{2.19}$$

A-line separating clay (C) from silt (M);

$$PI = 0.9(w_L - 8) \tag{2.20}$$

U-line approximately representing the upper limit for the plot of natural soils;

there is a fifth crosshatched area above the A-line and between PI values of 4 to 7, defining an area of silty-clays (CL-ML).

Figure 2.13 shows the USCS for the inorganic fine-grained materials.

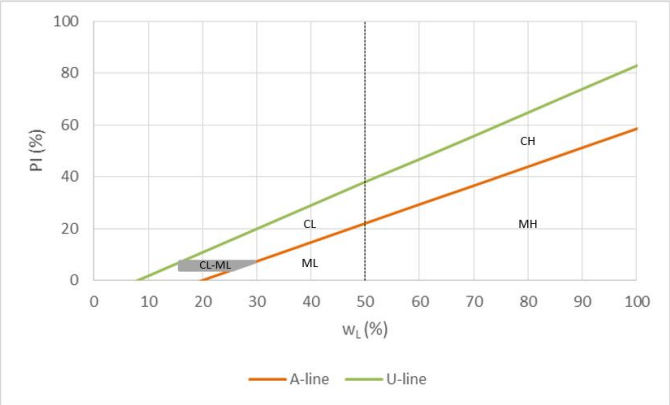

Figure 2.13: *USCS plasticity chart*

According to their plasticity and their liquid limits, soils are differently labelled (USDA-SCS, 1990):

clays with a high liquid limit (CH) - fat clays

silts with a high liquid limit (MH) - elastic silts

clays with a low liquid limit (CL) - lean clays

silts with a low liquid limit (ML) - silts

By plotting the estimated values of plasticity index **PI=351.25%** and liquid limit $\mathbf{w_L}$**=408.59%**, the studied bentonite belongs to the fat clays, that is inorganic clays with high plasticity (*Figure 2.14*).

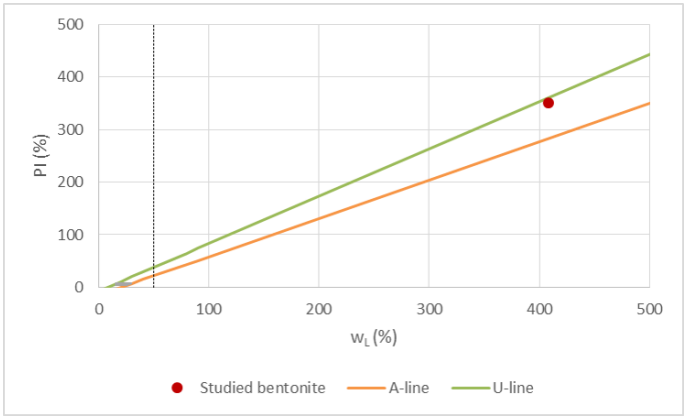

Figure 2.14: *Experimental datum plotted in the plasticity chart*

This result is in agreement with the bentonite definition and also with its mineralogical composition: the analysed bentonite contains 80% of montmorillonite and, in fact, montmorillonite based soils lay immediately under the U-line (USDA-SCS, 1990).

2.5.4 Other indexes

The natural state condition of the material in the laboratory environment is described, in terms of Atterberg limits, by the **liquidity index LI**, used for scaling the natural water content of the soil to the Atterberg limits:

$$LI = \frac{w - w_P}{PI} \tag{2.21}$$

It is equal to **-0.13** for the analysed material.

Another considerable index is the **consistency index CI**:

$$CI = \frac{w_L - w}{PI} = 1 - PI \tag{2.22}$$

As regards the mechanical behaviour, the latter one has for the fine-grained soils a role similar to the relative density for the coarse-grained ones: in fact, an increase in shear strength and stiffness and a decrease in the compressibility are associated to an increase in the Consistency Index. The value estimated for the studied bentonite is equal to **1.13**, corresponding to a solid-semisolid consistency; the *Table 2.9* describes different values of consistency of a soil.

The plasticity index depends not only on the clay percentage, but also on the mineralogy and on the kind of adsorbed cations: the **activity index A** takes into account these factors and it is related to the structural complexity of the minerals (Skempton, 1953). It specifically concerns the specific surface area controlling how much moisture is required to move a soil from one physical state to another one: high activity means large volume change during wetting and

Table 2.9: *Description of clay consistency*

IC values	**Consistency**
< 0	fluid
$0 \div 0.25$	plastic-fluid
$0.25 \div 0.50$	plastic-soft
$0.50 \div 0.75$	plastic
$0.75 \div 1$	plastic-solid
$\mathbf{> 1}$	**solid-semisolid**

large shrinkage during drying. It is defined as the ratio between the plasticity index PI and the clay fraction, both expressed in percentage:

$$A = \frac{PI}{CF} \tag{2.23}$$

It is equal to 4.82 for the studied bentonite, that means an active soil. This value is consistent with the hypotheses of Na-montmorillonite made in *chapter 2.1*: in wider terms, montmorillonite has high activity level; but a Na-montmorillonite has very high activity indexes (up to 7.2), while a Ca-montmorillonite reaches lower values (Samuels, 1950).
A further classification has been drafted according to the activity index (Skempton, 1953), as listed in *Table 2.10*.

Table 2.10: *Description of clay activity level*

A value	**Activity level**
< 0.75	inactive clays
$0.75 \div 1.25$	normal clays
$\mathbf{> 1.25}$	**active clays**

2.6 Comparison with known bentonites

Starting from data assessed so far, it is possible to compare the studied bentonite with other bentonite-based materials analysed in the literature; more precisely, the comparison is made with the bentonites most widely studied in Europe in the context of deep geological repository: the FEBEX bentonite, the MX-80 bentonite and the FoCa bentonite (Villar, 2004).
The *Table 2.11* allows to compare the three commercial well-known products with the studied material, according to what shown in the previous sections.

By comparing the reported values, the commercial product that is more similar to the studied one is the MX-80 bentonite: they have a similar mineralogical composition for most of the constituents; moreover, they have the same main exchangeable cation (Na), which produces a high activity index (as verified in both cases). Also the Atterberg limits and the clay fraction, which analytically determine the activity index, have the same order of magnitude.
The MX-80 bentonite is an active clay mostly composed by sodic montmorillonite; it is a worldwide known material implemented as backfilling and sealing body in disposal concepts in Sweden, Finland, Germany and France (Villar, 2004).
Henceforth, given the similarity between the two, it will be referred to the MX-80 bentonite for those parameters useful to the study but unworkable to determine experimentally.

Table 2.11: *Comparison between different kinds of bentonite*

		FEBEX bentonite	**MX-80 bentonite**	**(FoCa) bentonite**	**Studied bentonite**
Mineralogical composition	**Montmorillonite (%)**	80.5±3	65-82		80
	Illite (%)	11.5±3			
	Kaolinite (%)			44	4
	Ca beidellite (%)			44	4
	Quartz (%)	2±1	4-12	6	11
	Cristobalite (%)	2±1 (opal-CT)	small quantity		3
	Plagioclase (%)	2±1			
	Feldspars (%)	small quantity (K)	5-8		
	Calcite (%)	small quantity	small quantity	2	2
	Goethite (%)			6	
	Others (small quantities)		pyrite	hematite, gypsum	
	Main exchangeable cations	Ca, Mg	Na	Ca	Na
	Particle density (kg/m^3)	2'700	2'820	2'680	2'740
	Clay fraction (%)	67±3	80-90	75	73
Atterberg limits	**Liquid limit (%)**	102±4	350-570	98-112	408.59
	Plastic limit (%)	53±3	70	33-50	57.33
	Activity Index	0.73	3.11-6.25	0.64-1.05	4.82

Chapter 3

Hydraulic properties

The water transfer inside the bentonite buffer is basically due to the head gradient, according to the Darcy's law:

$$\frac{Q}{A} = k_{rw}\frac{\Delta h}{L} \tag{3.1}$$

where:

Q is the flow rate;

A is the section area, crossed by the water flow;

k_{rw} is the relative permeability coefficient;

$\Delta h/L$ is the hydraulic gradient, that is the ratio between the head difference Δh and the flow path L (height of the sample under the hypothesis of vertical flow).

The head gradient can be imposed by the suction exerted by the unsaturated bentonite or by the regional hydraulic properties. Suction Ψ is an important quantity in unsaturated soils: it is defined as the potential in pure water causing the same free energy at the same temperatures as in the soil water. It is worked out as the sum of three different terms:

$$\Psi = \Psi_g + \Psi_m + \Psi_s \tag{3.2}$$

where:

Ψ_g is the *gravitational potential*, corresponding to the hydraulic head;

Ψ_m is the *matrix* or *capillary suction*, defined as «the work per unit quantity of water to transport reversibly and isothermally an infinitesimal quantity of water to the soil from a pool containing a solution identical in composition to the soil water at the same elevation and external gas pressure as that of the considered point» (Mitchell, 2005);

Ψ_s is the *osmotic suction*, defined as «the work per unit quantity of water to transport reversibly and isothermally an infinitesimal quantity of water from a pool of pure water at a specified elevation and atmospheric pressure to a pool containing a solution identical in composition to the soil water, but in all other respects identical to the reference pool» (Mitchell, 2005).

This chapter focuses on the the main hydraulic properties governing the water flow in benonite buffer: the water retention capacity and the permeability.

3.1 Soil Water Retention Curve

The soil-water retention curve (SWRC) is of great interest in unsaturated soil engineering applications; in the context of deep geological repositories for nuclear waste, it is required for predicting the behaviour of bentonite barriers, as suction changes generally entail significant changes in hydro-mechanical characteristics.
The **soil-water retention curve** represents the relationship between the matrix suction, henceforth defined as **s**, and a measure of the water quantity in the soil, expressed by one of the parameters listed below:

the gravimetric water content **w** (%), described by the *Equation 2.10*;

the saturation degree **Sr**;

$$Sr = \frac{V_w}{V_v} \tag{3.3}$$

the volumetric water content $\boldsymbol{\theta}$;

$$\theta = Sr * n = \frac{V_w}{V} \tag{3.4}$$

where:

V_w is the volume of water contained in the soil

V_v is the volume of voids space

V is the total volume considered

n is the porosity, defined as the ratio between voids space and total volume.

In this study, both saturation degree and gravimetric water content trends have been investigated.
In order to reproduce the in-situ conditions of the engineered bentonite barriers, two different procedures can be implemented: a first one, under free swelling conditions and a second one, not adopted in this study because of instrumental and time limitations, in isochoric conditions. Because of the unavoidable presence of technological gaps between the engineered barrier and the host rock, the bentonite initially swells in unconfined conditions; when the contact is reached and the gaps are filled, it swells under confined conditions (Gatabin, 2016).

Examining *Figure 3.1*, it is possible to observe two different curves for the same porous samples: the blue one, corresponding to the drying path, and the green one, to the hydration path. In fact, the relation between suction and water content is not biunivocal, but the water content relative to a given suction depends on its previous water history (Delage, 2015). The The two different paths are due to the material pore size distribution: the more the void space dimension is heterogeneous, the more the difference between the two paths is accentuated. This is due to the different water path in parallel connection, the bottleneck effect in series connection and the drop effect causing different drying and wetting contact angles to the solid structure (*Figure 3.2*).

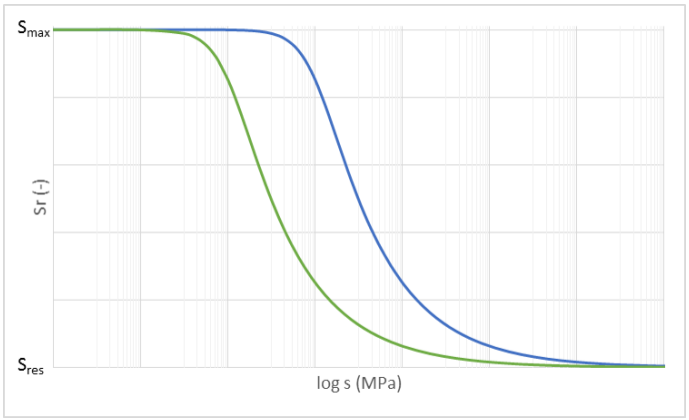

Figure 3.1: *Theoretical soil-water retention curve*

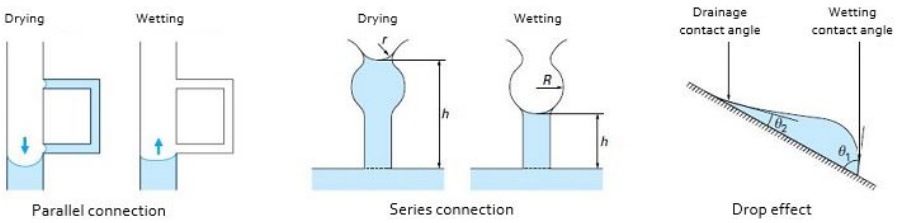

Figure 3.2: *Effects causing the hysteresis in the soil-water retention curve, picture modified from Delage, 2015*

3.1.1 Experimental determination of the SWRC

In order to trace the soil-water retention curve, it is important to be able to control the applied suction and to measure the corresponding water content: each couple of values represents a point in the SWRC; by repeating the measurement with different suctions, the whole curve is drawn.
Whereas the water content is a posteriori determined by weighing or calculating the sample volume, depending on the expression of the water content that is considered, the suction assessment is less immediate and more complicated. Different suction control techniques are available: since the university laboratory holds desiccators controlling suction through the *vapour equilibrium technique*, this method has been implemented. It is generally observed that the time required by samples to reach equilibrium is about one to two months, because of the low permeability of bentonite (Tang, 2005): in order to reduce times and costs, several desiccators will be used, controlling different suctions.
In order to understand whether the obtained points lay on the wetting or on the drying path, it is sufficient to observe the final gravimetric water contents: if they are higher than the initial one, the measures belong to the wetting path; otherwise, to the drying path.

Materials

The following apparatus is needed:

- saturated saline solution, as many as the number of different suctions desired;
- cups containing the samples;
- a support for each cup, guaranteeing the maximum contact surface of the sample with the atmosphere;
- desiccators, at least as many as the number of available saline solutions ;
- thermo-hygrometric sensors;
- precision scale (0.01 g);
- thermostatically controlled drying oven, capable of maintaining temperatures of 110±5°C for drying moisture samples;
- precision calliper.

Cups with the Petri dishes shape have been used, to avoid any mass loss: in fact, in unconfined cases, bentonite samples under a high relative humidity can swell considerably, show some fractures and lose some mass; the cup assures the containment of the whole mass. This is important to accurately calculate the water content after the end of the test. Little portions of the mass can also be lost during the volume measurement, by applying a too high pressure with the calliper.
Moreover, some little plastic bars of different shapes (according to their supply), have been used as support for the samples, given the unavailability of specific tools: these are important to assure the most possible uniform absorption of the

(a) *Bars used as support*

(b) *Desiccator containing the cup with the bars and the sample; thermo-hygrometric sensor taking measures*

Figure 3.3: *SWRC devices (pictures by Sara Rozzoni)*

relative humidity by every part of the samples. In absence of the bars, the sample would lay directly on the basis of the cup, and thus the lower surface would not play any role in reaching an equilibrium with the surrounding atmosphere, and in changing the sample volume and mass.
The sensor has been setted in order to take a measure every 2 hours, according to its memory size and to the total time period considered for this test. The Figure 3.3 shows the specific apparatus for the implemented technique.

Method

The *vapour equilibrium technique* is based on *Kelvin's law* (3.5), expressing the suction value s as a function of the relative humidity h:

$$s = u_a - u_w = -\frac{\rho_l RT}{M} \ln h \tag{3.5}$$

where:

u_a is the air pressure

u_w is the water pressure

g is the gravitational acceleration (g=9.81 m/s^2)

R is the molar gas constant (R=8,314 J mol^{-1} K^{-1})

T is the thermodynamic temperature (K)

M is the molar mass of water (M=18,016 g mol^{-1})

h is the given relative humidity (-).

Since suction is a function of temperature, desiccators have been placed within an environmentally controlled room, with a temperature of 20°C (±1°C) measured over time by thermohygrometrical sensors placed in the desiccators. The procedure requires that the sample of compacted bentonite is placed in a confined atmosphere in a desiccator under a controlled humidity: the humidity is controlled through a saturated saline solution installed at the basis of the desiccator; the water exchange occurs through the vapour phase till the equilibrium of the relative humidity (Delage, 2015). Mechanical and hydraulic equilibria are reached simultaneously: this can occur after a time period, that directly depends on the sample size and on the desired suction (*i.e* the relative humidity). Equilibrium is reached when both the relative humidity, the sample mass and volume are constant. In the present study, it has been detected experimentally by weighing the samples every two weeks, in order to perturb as little as possible the controlled atmosphere: stabilisation was assumed when the change in mass with time was lower than a threshold $\frac{\Delta w}{\Delta t} < 0.5 \times 10^{-3} min^{-1}$, in agreement with to Gatabin et al. (2016); once this criterion is met, the test was stopped. The *Figure 3.4* shows the equilibrium time for different relative humidities.

Although data are quite scattered, they clearly show a linear trend in a semi-

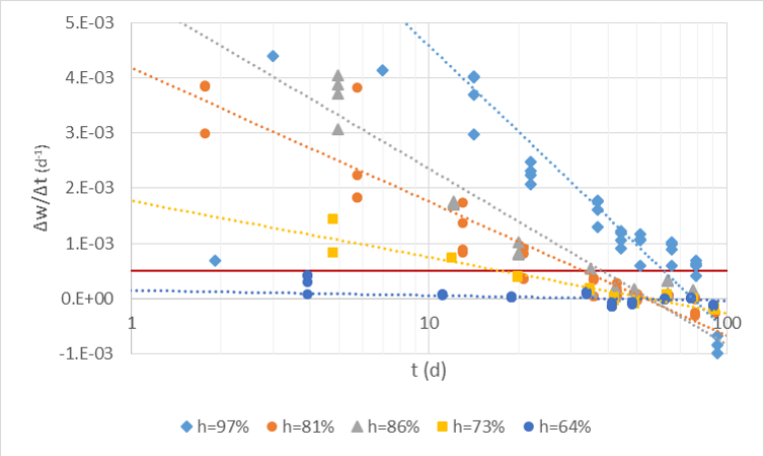

Figure 3.4: *Determination of the equilibrium time through a threshold criterion*

logarithmic plane: the equilibrium time has been calculated where the linear regression intersects the given threshold. Negative data occur after the stabilisation, when the sample can show little shrinkage; however, they are in modulus lower than the threshold. For the samples with a target moisture of 64%, there are not considerable changes in mass: this could suggest an initial relative humidity of the sample close to the target one; this point is deeply analysed in 3.1.1. Data show a linear correlation between the actual moistures and the equilibrium times (*Figure 3.5*), listed in the *Table 3.1.* Moreover, this points out the theoretical relative humidity value (Delage, 2015) and the real one; this one is measured over time by a thermohygrometrical sensor. *Table 3.1*
shows a good approximation between the two values, except for the zinc sulfate solution ($ZnSO_4$): this difference could be due to some impurities in the saline solution.

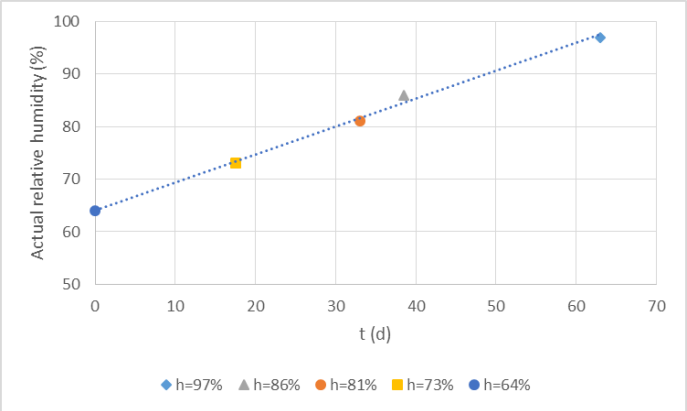

Figure 3.5: *Linear relation between actual relative humidities and equilibrium times*

Table 3.1: *Relation theoretical-effective relative humidity, suction, and equilibrium time, in saturated saline solutions*

Saline solution	**Theoretical relative humidity (%)**	**Actual relative humidity (%)**	**(Suction) (MPa)**	**Equilibrium time (d)**
K_2SO_4	97.0	97.0	4.11	63
$ZnSO_4$	91.3	81.0	28.46	33
KCl	86.0	86.0	20.37	38.5
NaCl	76.0	73.0	42.50	17.5
NH_4NO_3	65.0	64.0	60.27	$\rightarrow$0

The experiment has been performed by using samples of compacted bentonite, with an average diameter of 51 mm and an average height of 13 mm. 40 g of bentonite in powder have been compacted at the oedometer to a maximum pressure of 4.79 MPa (the fabrication process is better explained in *Section 4.1*): after compaction, the samples have been carefully removed from the oedometric mould and placed in cups with larger diameter, to assure free swelling conditions. The average density of the compacted samples before their positioning in the desiccators is equal to 1'482 kg/m^3, and their water content is equal to 12.4%.
Precisely, ten desiccators have been used for five different solutions: two for each of them.
In the smallest ones, only one sample has been placed: this is the more accurate measurement, because the relative humidity is directly measured by the sensor. In order to guarantee the repeatability and thus the validity of the results, other three samples and an empty cup with the bars have been put in the largest desiccators (*Figure 3.6*): the further three samples help to calculate an average value, while the empty cup helps to verify that there is not moisture absorption by the support. If there was any important change in mass, it would have meant an absorption by the cup and the bars, and that value should have been deducted from the sample gross mass. In this case, there were no absorption by the cup and the bars.

Figure 3.6: *Desiccator with three samples and an empty cup (picture by Sara Rozzoni)*

Whereas the gravimetric water content w is directly defined by weighing the sample before and after its drying in the oven (*Equation 2.10*), the degree of saturation Sr needs the determination of the sample volume: this represents an important issue in free swelling conditions tests. That is the reason why the cylindrical shape has been chosen for the samples; thus, their volume is easily calculated from the measurements of the height and the diameter by a precision calliper (Gatabin, 2016). The degree of saturation is finally worked out as:

$$Sr = \frac{V_w}{V_v} = \frac{V_w}{V - V_s} = \frac{\frac{M_w}{\rho_w}}{V - \frac{M_s}{\rho_s}} \tag{3.6}$$

where:

V_w is the volume of water contained in the soil,

V_v is the volume of voids space,

V is the total volume considered,

V_s is the solid volume,

M_w is the mass of water contained in the soil,

ρ_w is the water density, equal to 1'000 kg/m^3,

M_d is the dry mass of the sample, calculated through the (2.10),

ρ_s is the particle density, equal to 2'740 kg/m^3.

Imprecisions are unavoidably introduced in the saturation degree determination, while the gravimetric water content has only an instrumental error, depending on the precision scale.
The model used for the interpretation of the soil-water retention data is the *Van Genuchten model*:

$$Sr = S_{res} + (S_{max} - S_{res})\Big(1 + \Big(\frac{s}{CSR1}\Big)^{CSR2}\Big)^{-(1-\frac{1}{CSR2})} \tag{3.7}$$

where:

Sr is the degree of saturation (-)

S_{res} is the residual degree of saturation, imposed equal to 0

S_{max} is the maximum degree of saturation, imposed equal to 1

s is the suction (Pa)

$CSR1$ (Pa) and $CSR2$ (-) are empirical constants, derived from the model calibration.

Experimental results

The water retention curve obtained from the five different saline solutions is shown in *Figure 3.7*. Experimental data are also qualitatively and quantitatively in line with the water retention curve of compacted MX-80 bentonite/sand mixture, determined by Gatabin et al. (2016). This supports what discussed in 2.6, regarding the similarity between the studied soil and the MX-80 bentonite; now, it is possible to affirm that the two materials have not only similar mineralogical composition and plastic behaviour, but also a similar sorption curve in unconfined conditions. It is coherent, because the latter one depends on the clay fraction and on the plasticity index of the soil (Delage, 2015).
The error bars in *Figure 3.7* show the error given by averaging the four samples for each desired suction: the one in the smaller desiccator and those in the bigger. Since an average error of 2% has been measured between the relative humidities in the small and in the big desiccators for the same saline solution (probably due to their different size), also the calculated water content w is

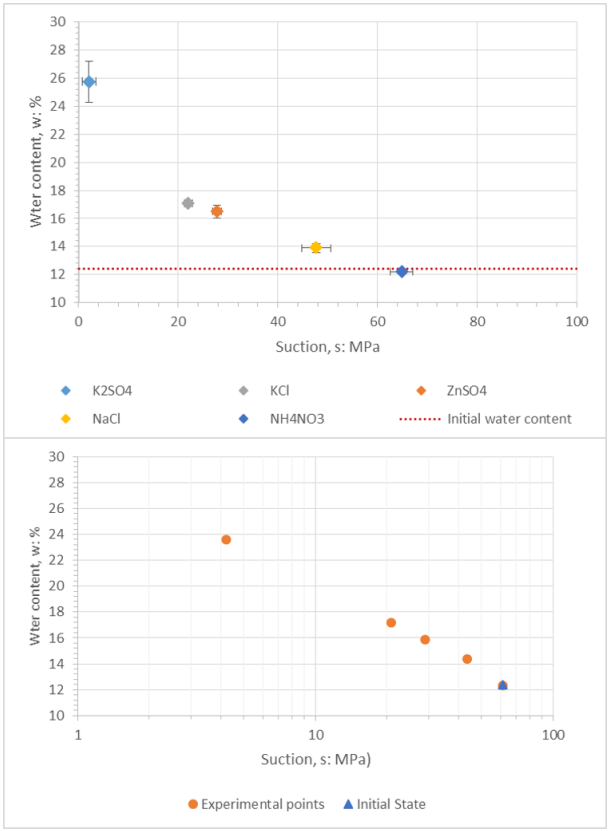

Figure 3.7: *Water retention curve expressed in terms of gravimetric water content versus suction. Each point corresponds to a different sample*

different. The smallest suction datum deserves some comments, as it shows a large vertical error bar: this is explained by the fact that for the same difference in suction, the difference in water content is much higher for low suction, as it can be easily deduced from the typical sorption curve shape. Thus, since the four samples are subjected to a suction of 64% lower than the others, they show greater differences in water content.

By regarding the *Figure 3.7*, it is possible to note that the gravimetric water content w of the samples at the highest suction (w=0.122) is close to the one of the initial state (w=0.124). This means that the initial suction of the compacted bentonite is close to 62 MPa. Moreover, a water content lower than the initial one should entail a reduction in mass and volume, because the experimental point would belong to the drying path. This is not verified in this study; on the contrary, for a reduction of the water content of 1.6%, the samples show a little increase in mass (0.07%) and volume (2%). Whereas the gravimetric strain can be neglected, the volumetric one can be explained as the result of a little shrinkage (negative deformation) due to a little moisture loss, and the positive elastic strain following the unloading phase, after the oedometric compaction. Thus, by assuming an initial suction slightly higher than 62 MPa, the total strain for each sample is the joint result of two different effects: an elastic volumetric strain of the order of 2% and the strain due to the moisture absorption (or loss, depending on the path).

Although it is less accurate than the previous one, also the curve *degree of saturation versus suction* has been assessed. The *Van Genuchten model (3.7)* allows to draw a soil water retention curve, under the hypothesis of a constant void ratio. The model parameters have been arbitrarily chosen in order to let the experimental data lay on the curve.
In free swelling conditions, it is physically impossible to maintain the void ratio constant: *Figure 3.8* presents the different values of the void ratio, validating the laying of points at different suction on different sorption curves. An important decrease in the air entry pressure is associated with an important swelling of the material (Dieudonné, 2016): in fact, a higher void ratio means more linked voids and this explains a decrease in the air entry pressure.

Lastly, the total volumetric, axial and radial strains developed by the sample at different suctions are shown in *Figure 3.9*, in order to detect a possible anisotropy: in fact, the axial strains are more than twice the radial ones. This anisotropy is explained by the uniaxial compaction method, which induced a preferential orientation of the clay particles in the horizontal plane; this result is in line with the study made by Gatabin et al. (2016). The experimental data in *Figure 3.9* clearly show the joint effects of two different kinds of strain, as explained before. The *Figure 3.10* shows the same data, cleared from the elastic strains by subtracting them.

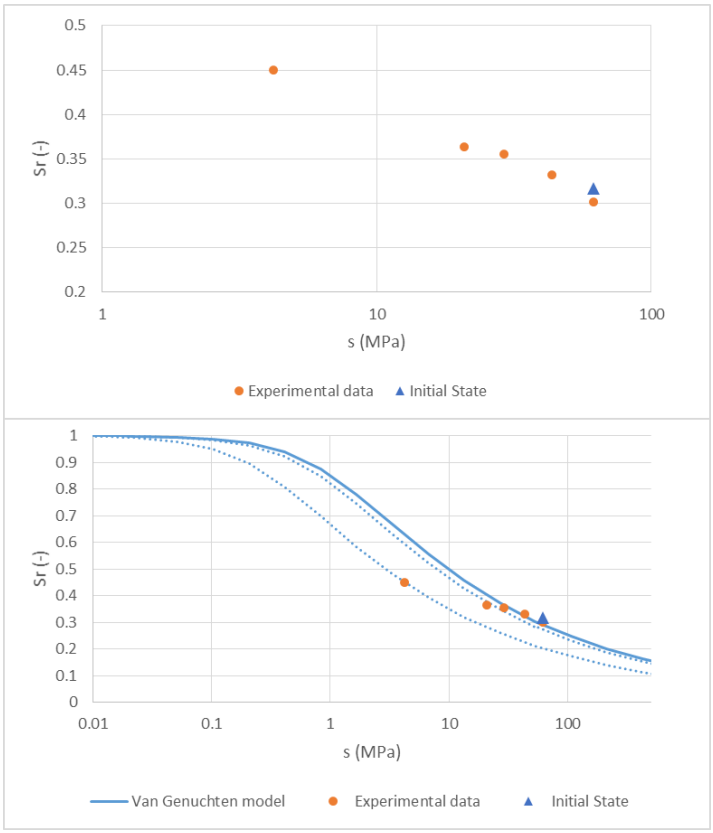

Figure 3.8: *Water retention curve expressed in terms of degree of saturation versus suction, as a function of the void ratio*

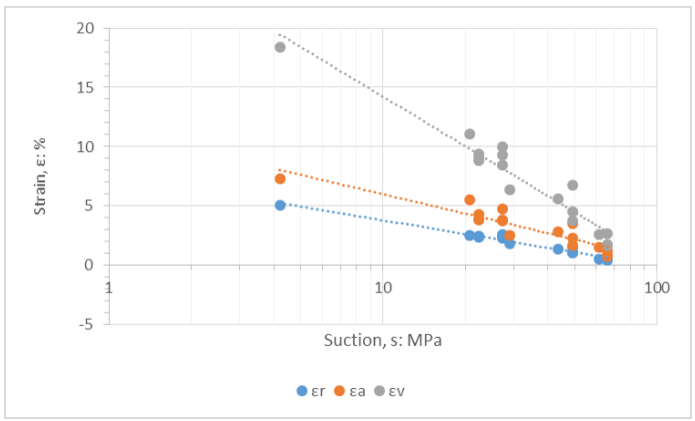

Figure 3.9: *Relationship between the volumetric, axial and radial strains and suction for the unconfined samples*

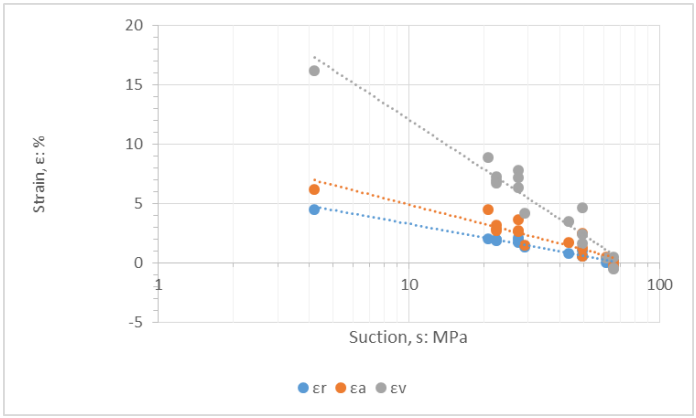

Figure 3.10: *Relationship between the volumetric, axial and radial strains and suction for the unconfined samples, cleared from the elastic strain effect*

3.2 Permeability coefficients

One of the characterising properties of high density compacted bentonite for its implementation in nuclear waste storages is its permeability: compacted bentonite has very low permeability, a feature which plays a fundamental role in reducing groundwaters percolation. In fact, the hydrogeological transport is the main radionuclide transfer mechanism (Villar, 2004).
In order to experimentally determine the permeability coefficient, two different methods have been executed in the laboratory: a falling head permeability test and a consolidation test. They provide the estimation of the **permeability to water k** of the bentonite, that is the mean velocity of water flow in porous materials under prescribed flow conditions. Starting from it, the **intrinsic permeability K** can be estimated, through the (*3.8*). Whereas the first one depends on the experimental conditions, the latter one is an intensive property depending only on the material structure:

$$K = k\frac{\mu_w}{\rho_w g} \tag{3.8}$$

where:

μ_w is the dynamic viscosity of the fluid, water in this case, and it is equal to 0.001 Pa·s

ρ_w is the fluid density, equal to 1'000 kg/m^3

g is the gravitational acceleration, 9.81 m/s^2

In this study, both permeability coefficients have been assessed and compared to data from literature.

3.2.1 Materials

Two different tests have been performed on two samples of bentonite preliminarily compacted. Both tests have been executed in the oedometric cell: in order to detect the height changes, this was equipped with two precision dial gauges (0.01 mm). Since the sample conditions have to be as much as possible stationary (neither consolidation nor swelling occurring), a constant load equal to half of the preconsolidation pressure p_c has been applied to the sample during the hydration phase. In fact, with a higher load, the stabilisation under hydration would have been reached later; with a smaller one, some swelling effects could have developed: if this happened, permeability estimation would be misrepresented because a bigger volume means a bigger void ratio, that is an easier water flow and so an overestimated permeability value.
In order to guarantee the water flow, two porous stones have been placed in the upper and lower parts of the oedometric ring. A graduated tube with small diameter, passing though the basis of the oedometer, has been filled with water up to an initial height h_0 from one side, and closed by a clamp from the other side; thus, the water passed through the sample through its bottom.

3.2.2 Falling head permeability test

Method This test is usually performed on saturated samples, in order to assess the permeability coefficient in fine-grained soils.
The graduated tube linked to the oedometric cell allowed to monitor the hydraulic head as function of time: these are fundamental quantities acting in the *Darcy's law* (3.1), on which this test is physically based.
By assuming a head difference equal to h in a certain time period t, and by rewriting the flow rate Q as the water volume leaving the tube of a area in a time period dt,

$$Q = -a\frac{dh}{dt} \tag{3.9}$$

for the water mass balance the *Darcy's law* becomes:

$$\frac{dh}{dt} = -k\frac{A}{a}\frac{h}{L} \tag{3.10}$$

By integrating it with the initial condition (h=h_0 at t=0), the permeability coefficient k can be assessed:

$$ln\left(\frac{h_0}{h}\right) = k\frac{A}{aL}t \tag{3.11}$$

Experimental results

The sample has been compacted at the oedometer up to a density ρ of 1'497 kg/m^3 by a pressure p_c of 4.79 MPa. It has been assumed saturated when the height stabilisation was reached; in the present study it occurred more than one week from the beginning of hydration. The void ratio e during the test duration was equal to 1.08.
The permeability k can be experimentally estimated through the *Figure 3.11*:

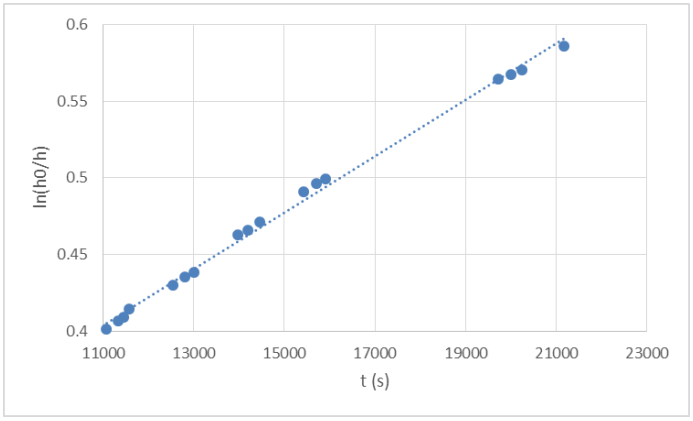

Figure 3.11: *Linear regression for the estimation of the permeability*

it presents the experimental data obtained by following the falling head test procedure, for a stabilised height of the sample. The graph is constructed with the time t as abscissa and the natural logarithmic of the ratio h_0/h as ordinate; the permeability k is easily obtained by multiplying the angular coefficient of

the traced curve times the ratio aL/A.
The falling head test provides an estimation of the permeability k equal to $\mathbf{4.08 \cdot 10^{-11}}$ **m/s**, corresponding to an intrinsic permeability of $\mathbf{4.16 \cdot 10^{-18}}$ $\mathbf{m^2}$.

3.2.3 Consolidation test

Method Another method for the estimation of the permeability is through a consolidation test.
If submitted to a static load, soils expel water from the pores and dissipate the water pressure u; in fine-grained soils, because of their low permeability, this process is delayed, and thus the volumetric strain. This phenomena, characterised by a load-strain-time relation, is called **consolidation** (Terzaghi, 1943).
The *Terzaghi's oedometric consolidation theory* assumes the following simplifying hypotheses:

one-dimensional consolidation (*i.e.* vertical filtration and vertical strain);

uncompressible water and soil particles (*i.e.* constant ρ_w and ρ_s);

Darcy's law (3.1) validity, reasonable hypothesis since the fine-grained soils are characterised by laminar flow;

saturated, homogeneous and isotropic soil over time, with constant permeability in time and space, and elastic-linear stress-strain behaviour;

effective stress principle validity, assessing that the effective principal stress σ' corresponds to the difference between the total principal stress σ and the pore water pressure u (Terzaghi, 1943).

Under these hypotheses, the *general flow equation* (3.12) can be rewritten as below:

$$k_x \frac{\partial^2 h}{\partial x^2} + k_y \frac{\partial^2 h}{\partial y^2} + k_z \frac{\partial^2 h}{\partial z^2} = \frac{1}{1+e}\Big(e\frac{\partial S_r}{\partial t} + S_r \frac{\partial e}{\partial t}\Big) \tag{3.12}$$

$$k_z \frac{\partial^2 h}{\partial z^2} = \frac{1}{1+e}\frac{\partial e}{\partial t} \tag{3.13}$$

Through some expedients and by introducing the *compressibility coefficient*

$$a_v = -\frac{\partial e}{\partial \sigma'_v} \tag{3.14}$$

the equation becomes:

$$\frac{k_z(1+e)}{a_v}\frac{\partial^2 h}{\partial z^2} = -\frac{\partial \sigma'_v}{\partial t} \tag{3.15}$$

By rewriting both the head term h (*3.16*) and the stress term σ (*3.17*) as a function of the *excess water pressure* u_e resulting from the load application σ'_v,

$$\frac{\partial^2 h}{\partial z^2} = \frac{1}{\gamma_w} \cdot \frac{\partial^2 u_e}{\partial z^2} \tag{3.16}$$

$$\frac{\partial \sigma'_v}{\partial t} = \frac{\partial \sigma_v}{\partial t} - \frac{\partial u_e}{\partial t} \tag{3.17}$$

the continuity equation in Terzaghi one-dimensional consolidation is equal to:

$$\frac{k_z(1+e)}{\gamma_w a_v}\frac{\partial^2 u_e}{\partial z^2} = \frac{\partial u_e}{\partial t} \tag{3.18}$$

where the term

$$\frac{k_z(1+e)}{\gamma_w a_v} = \frac{k_z}{\gamma_w m_v} = c_v \tag{3.19}$$

is the *vertical consolidation coefficient*. This is a function of the permeability to water k, of the water specific weight γ_w and of the volumetric compressibility coefficient m_v. The latter parameter is determined by an oedometric test, and it is equal to the ratio between the axial strains developed and the loading step applied:

$$m_v = \frac{\Delta\varepsilon_a}{\Delta\sigma'_v} \tag{3.20}$$

Another formulation for the vertical consolidation coefficient is

$$c_v = \frac{T_v H^2}{t} \tag{3.21}$$

where:

H is the drainage height, equal to the maximum path covered by a water molecule to leave the sample: in the present study it is equal to a half of the sample height, because the water can comes out from both the lower and upper layers;

T_v is a time factor, equal to 0.197 for a consolidation rate of 50%.

Thus, the permeability coefficient has been estimated through the (3.19).

Experimental results

The used sample has been compacted with the loading frame, up to a density ρ of 1'881 kg/m^3 by a pressure p_c of 35 MPa. The loading step 2.39 MPa - 4.79 MPa has been investigated: the load has been applied after hydrating for one week, by assuming the saturation of the sample. The void ratio e at the end of the consolidation process was equal to 0.72.

Volumetric compressibility coefficient $\mathbf{m_v}$ The axial strain occurring in correspondence to the application of the load $\Delta\sigma'_v$ equal to 2.39 MPa has been monitored; the coefficient m_v, determined by the (*3.20*), is equal to $\mathbf{1.06 \cdot 10^{-2}}$ **MPa^{-1}**.

Vertical consolidation coefficient $\mathbf{c_v}$ The *Casagrande method* has been applied in order to experimentally determine the *vertical consolidation coefficient* c_v. The sample height has been measured in different time periods (*Figure 3.12*); a graph is constructed with the logarithm of time as abscissa and the height as ordinate. The results are in line with the consolidation theory: they show a first part AB corresponding to the primary consolidation process (*hydrodynamic consolidation*) and a second one CD corresponding to the secondary compression process, induced by viscous strains (*creep*). Although the partition

is not tidy, because a little part of the secondary compression is present in the primary one and vice versa, an assumption of clear partition is made.
In order to calculate the drainage height, corresponding to half of the average

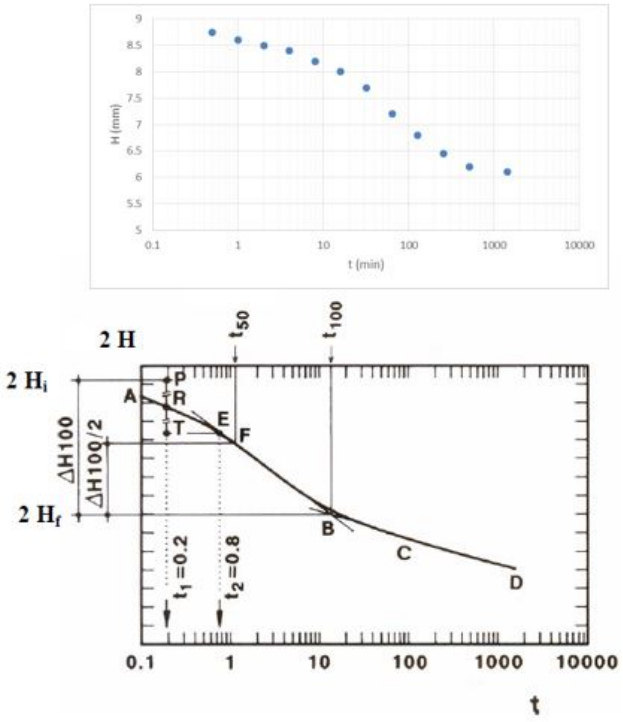

Figure 3.12: *Consolidation curve*

height of the sample during the consolidation process $H_d = \frac{H_{50}}{2} = \frac{H_i + H_f}{4}$, it is necessary to estimate the correct initial height: by assuming that the curve is a parabola for average consolidation rate U_m smaller than 60%, the ratio of the height variations *s(t)* at different times is equal to the square root of the ratio of the two times,

$$\frac{s(t_1)}{s(t_2)} = \sqrt{\frac{t_1}{t_2}}, \tag{3.22}$$

assumed t_1 small enough and t_2=4t_1. By overturning the segment RT, equal to the retreat between t_2 and t_1 with respect to the point R, the corrected initial height is determined.
The final height is obtained by the intersection between the CD line, corresponding to the secondary compression, and the tangent line EB to the second tract of the primary consolidation.

The permeability estimated by *Equation 3.19* is $\mathbf{2.01 \cdot 10^{-13}}$ **m/s**, and the intrinsic permeability K is equal to $\mathbf{2.05 \cdot 10^{-20} m^2}$.

Discussion

The *Table 3.2* summarizes the results obtained by the two different tests.
By comparing the two tests, it is possible to observe a high difference in the

Table 3.2: *Comparison of the experimental results*

	Falling head test	**Consolidation test**
k (m/s)	$4.08 \cdot 10^{-11}$	$8.06 \cdot 10^{-13}$
K (m^2)	$4.16 \cdot 10^{-18}$	$8.21 \cdot 10^{-20}$
ρ (kg/m^3)	1'500	1'880
e (-)	1.08	0.72

permeability value: this is due to a different compaction pressure, which means different densities and void ratios. Since the intrinsic permeability K depends on the pore diameter of the material through the *Darcy's law* (3.1) and the *Poiseuille's law* (3.23), the decrease in the average diameter of the pores as density increases produces a permability decrease (Villar, 2004):

$$Q = \frac{\pi}{128} \frac{\Delta u}{\mu_w L} D^4 \tag{3.23}$$

where:

Q is the flow rate (m^3/s);

Δu is the difference of neutral pressure (Pa);

μ_w is the dynamic viscosity of the fluid, water in this case, and it is equal to 0.001 Pa·s;

L is the flow path (m);

D is the average pore diameter (m).

Moreover, the two tests have been performed at different loading conditions: the falling head test, with a constant load equal to 2.39 MPa; the consolidation test, with a load equal to 4.79 MPa, twice the first one. This can produce a better adherence between the sample and the oedometric ring and limit a preferential water flow, which would cause an overestimation of the real permeability value. As regards the permeability coefficient estimated through the consolidation test, considered the most reliable, this differs only of one order of magnitude from the literature data, presenting an intrinsic permeability of $\mathbf{8 \cdot 10^{-21}}$ (Gerard, 2008).

Chapter 4

Mechanical properties: swelling test

In order to design a nuclear waste repository, it is important to study the mechanical properties of the compacted bentonite, which play a fundamental role in determining its in-situ strength and deformability: the most relevant mechanical property, analysed in this chapter, is its tendency to swell, increasing its volume. This peculiar mechanical behaviour is due to the bentonite nature, since it is constituted mostly of smectites, the main responsible for the clay swelling capacity.

Three main factors affect the swelling capacity of a soil: a first one, linked to the intrinsic properties of the material, such as the kind and quantity of swelling minerals and adsorbed cations; a second one, depending on the saturation water characteristics; and a last one, is an external factor, that is the water availability, the soil stress history and the temperature (Villar, 2004).
It would be interesting to compare different bentonite-based materials at different thermo-hydro-mechanical conditions, in order to detect the relation between the swelling capacity and the above-cited variables. According to the laboratory devices, and given the unavailability of other bentonites, this chapter focuses on the volume change relating to different initial dry densities.

During its implementation in nuclear waste repositories, the compacted bentonite is placed under unsaturated conditions.
Due to its initial high suction (as discussed in 3.1), it takes water from the host rock; once hydrated, it experiences an initial unconfined swelling because of the unavoidable gaps between the buffer and the surrounding rock, defined as **swelling potential**. Then, it swells until the strains are prevented: the pressure developed against the rock under confined and saturated conditions is defined as **swelling pressure Sp** (Villar, 2004).

In order to reproduce the in-situ conditions, four swelling tests have been performed at the oedometer: the swelling test procedure is graphically represented below.

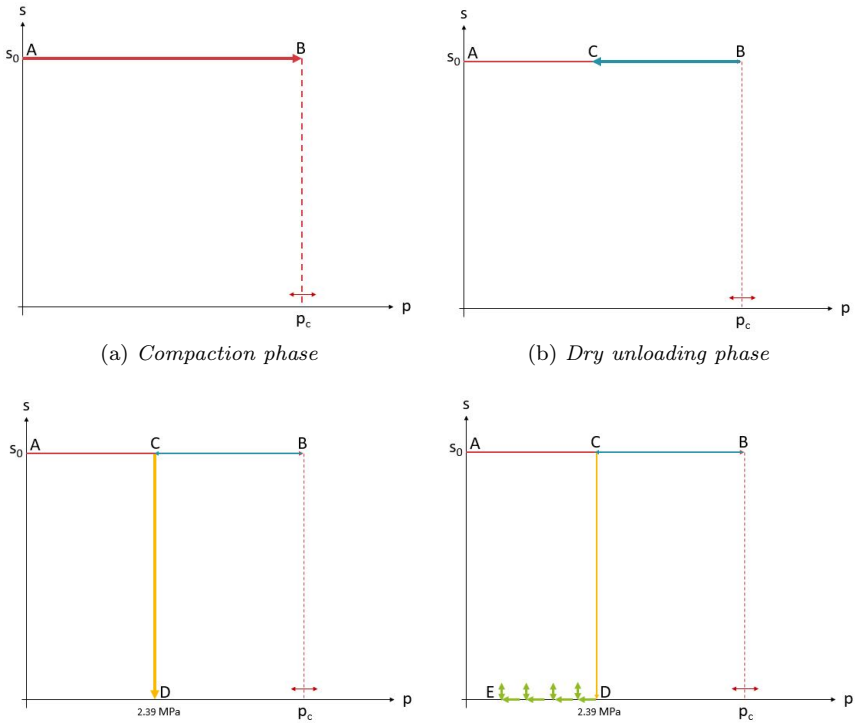

(a) *Compaction phase* (b) *Dry unloading phase*

(c) *Hydration phase* (d) *Hydrated unloading phase.*

Figure 4.1: *Swelling test procedure*

First of all, the established mass of powder bentonite has been compacted up to different densities, in order to guarantee the comparison between the results. Two different methods have been used: the loading frame and the oedometric cell; they allow to reach different preconsolidation pressures p_c, in order to obtain samples at different compaction rate. The suction can be assumed constant for the whole **compaction phase** (path AB in *Figure 4.1a*).
Each sample is unloaded at a constant pressure equal to 2.39 MPa at the oedometer, under constant-suction conditions: this is the **dry unloading phase** (path BC in *Figure 4.1b*).
Then, the samples have been hydrated under the previously applied constant pressure (path CD in *Figure 4.1c*): this is the **hydration phase**. They are assumed to be saturated (null suction s) at the end of this phase: the hypothesis has been made that the saturation is reached when the sample height reaches a constant value. The pressure value has been arbitrarily chosen, within the range pressure bearable from the oedometer.
Once assumed saturated, different unloading steps have been applied in order to allow the sample to swell (paths DE in *Figure 4.1d*). By doing it, the effective stress decreases, the void index e increases and the sample desatures; since the hydration is continuous from the beginning of the hydration phase up to the end of the test, the sample resaturates: this dual phenomenon is represented by the green arrows in the *Figure 4.1d*, each couple of arrows represents an unloading step (the number of arrows in the graph is indicative). The resultant swelling is the combined effect of two mechanisms: a first one, elastic, due to the mechanical unloading, which causes a bigger void index, that is an easier water flow; a second one, linked to the hydro-chemical characteristics of the smectites, due to their interaction with the water molecules penetrating into the sample. This latter phase, called **hydrated unloading phase**, allows to estimate the swelling pressure Sp.

4.1 Compaction and dry unloading phases

A static compaction method has been chosen, because of the available devices in the laboratory and, above all, because of the need of a sample as dry as possible, in order to better evaluate its swelling capacity with hydration. For this reason, other methods expecting the preliminary partial or total saturation of the sample are not suitable for this purpose.
In order to compact the bentonite powder, two different methods have been implemented: the oedometric cell and the loading frame. They both apply an uniaxial compaction on the soil. Although it would have been better to use an unique method to obtain more reliable and comparable results, both techniques have been implemented for the following reasons.
Since the further phases need the oedometric cell, it is preferable to compact the soil with it, in order to perturb the sample as less as possible. In fact, if it is compacted by the frame, it has to be carefully removed and replaced in the oedometric ring: this necessarily leaves a gap between the sample and the ring, wider than in case of an oedometric compaction, where the replacement is not necessary. Thus, a worse adherence can entail different test conditions and misrepresent the results; for example, in the loading frame case, the bentonite can swell sideways before, and vertically later.
On the other hand, by assuming that the bentonite has to be compacted at preconsolidation pressures higher than 4.79 MPa, the oedometer covers a little range of suitable pressures (4.79-5.75 MPa), which means a little range of bentonite densities. In contrast, the loading frame reaches higher values of pressure, that implies higher densities.
As the aim of this chapter is to study the trend of the swelling pressure with density, it has been chosen to neglect the different test conditions, and to use both methods depending on the desired dry density.

4.1.1 Materials and methods

In order to set up an oedometric swelling test, it is important to abide by some dimensional requirements during the compaction phase: a low height (**h**) of the sample and a high value of the ratio between the diameter of the sample and its height $\frac{D}{h}$, included between 2,5 and 6 (AGI, 1994). They both have the practical aim of reducing friction between the sample and the oedometric ring.
In order to reach the maximum compaction pressure, it has been chosen the ring with the minimum diameter available (50 mm) and the standard height (20 mm): the above-cited requirements are satisfied.
Usually, the sample has to be bigger than the ring, and this one is driven into the sample itself. For materials with low or intermediate consistency, such as bentonite powder, it is impossible to proceed in this way because of their texture. Therefore, the powder has been inserted in the ring, and then compacted (AGI, 1994).

Reliability test

Two compaction tests have been initially set up to evaluate their comparability: one at the oedometer and the other one at the loading frame. In both cases, two filter papers have been placed at the upper and lower surfaces of the sample to avoid mass leaks. As regards the stress strain boundary conditions imposed in the two devices, they equally entail an uniaxial vertical strain and a vertical load application: in the oedometer, this is inevitably a stepwise application, whereas in the loading frame it is a continuous one.
Figure 4.2 shows the needed materials and the procedure to compact the bentonite at the oedometer. The load has been increased manually from 0 to 4.79 MPa, and then decreased up to 0 MPa.
For the loading frame (*Figure 4.3*), the procedure is the same but in the frame cell; moreover, there are not the dial gauges, but a continuous displacement gauge. The load has been increased mechanically from 0 to 7.69 MPa and then decreased up to 0 MPa.

The two tests show consistent results: *Figure 4.4* presents the two paths in the same pressure range (0-4.79 MPa); results are presented in terms of dry density ρ_d, calculated as:

$$\rho_d = \frac{\rho}{w+1} \tag{4.1}$$

where ρ is the soil density, calculated as the ratio between the measured mass of the sample and its volume, and w is the gravimetric water content, equal to 0.124. At the loading frame, the sample reaches higher densities because it bears higher pressures. In both cases, the density increases in a non-linear way, in comparable paths for the two methods; during the unloading phase the decrease in density value is one order of magnitude lower.

Initial dry densities ρ_d

After the reliability test, the swelling test has been performed on four different samples. The *Figure 4.5* shows the relation between the preconsolidation pressure p_c and the initial dry density ρ_d: there is a semi-logarithmic relation between the two quantities: whereas at low pressure it is possible to cover wide range of densities, at high pressure it becomes smaller and smaller; this is physically reasonable.

Table 4.1: *Dry densities reached through the two different compaction methods*

	Preconsolidation pressure (MPa)	**Sample height (cm)**	**Initial dry density (g/cm^3)**	**Swelling Method**
1	4.79	1.38	1.29	Oedometer
2	5.23	1.29	1.33	Oedometer
3	15.28	0.83	1.53	Loading frame
4	76.39	0.74	1.71	Loading frame

After the compaction, both at the oedometer and at the frame, each sample has submitted to a pressure equal to 2.39 MPa at the oedometer, in order to

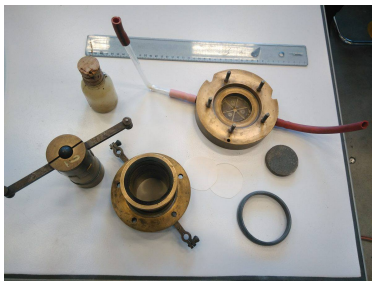

(a) *From left to right: piston, paraffin, cell body, filter papers, basis with drainage tubes, gasket, porous stone.*

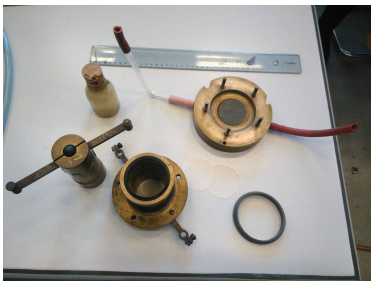

(b) *Porous stone into the basis to guarantee vertical drainage.*

(c) *Filter paper on the porous stone and gasket sealing the space between the body of the cell and the basis.*

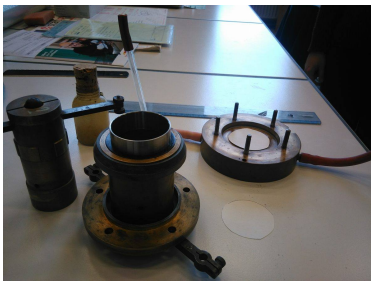

(d) *Ring in the cell body (greased by some paraffin to ease its insertion) .*

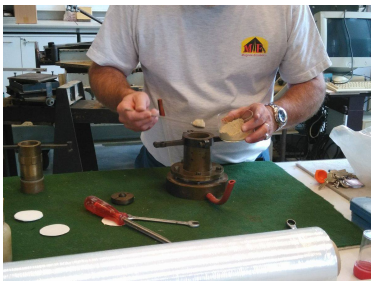

(e) *Cell body on the basis and bentonite filling .*

(f) *Piston in the cell body.*

(g) *Oedometric compaction - two dial gauges measure displacements.*

Figure 4.2: *Oedometric compaction (pictures by Sara Rozzoni)*

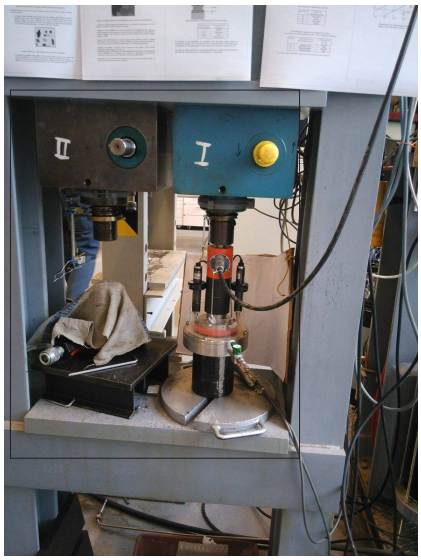

Figure 4.3: *Loading frame*

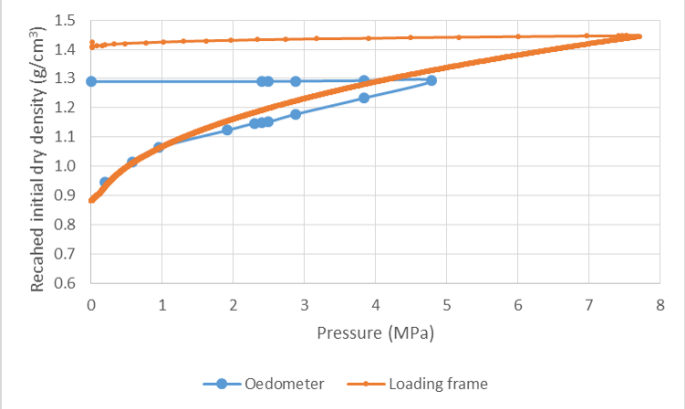

Figure 4.4: *Comparison between reached dry density through two different compaction methods*

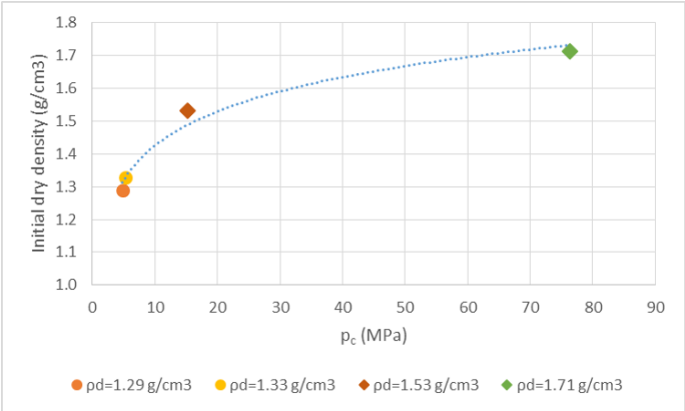

Figure 4.5: *Relation between preconsolidation pressure and reached dry density*

allow the bentonite to swell once hydrated. By unloading from the preconsolidation pressure to 2.39 MPa the samples experience an average elastic strain of 2%: the sample height and thus the dry density presented in *Table 4.1* are the ones after the elastic strain.
The applied pressure wants to qualitatively represent the host rock pressure exerted in in-situ conditions. From a quantitatively point of view, by assuming a rock specific weight γ of 20 kN/m^3, the applied load σ should have a order of magnitude of or greater than 10 MPa ($\sigma = \gamma h$), where the storage depth h is equal to 500-1000 m (Goguel, 1987). Unfortunately the available oedometer do not bear this pressure.
The two porous stones at the bottom and at the top guarantee the vertical drainage.

4.2 Hydration phase

The swelling test is performed on assumed saturated bentonite: so, the samples have been hydrated. The low permeability of compacted bentonite entails long period times for reaching the saturation: because of it, and because of time limitations, samples have been assumed saturated when their height was steady.
Depending on their initial compaction, their behaviour when in contact with water entirely changes, as shown in *Figure 4.6*. Two different responses are shown: swelling or collapse.
This dual behaviour substantially depends on the preconsolidation pressure of the samples, directly responsible for their density as shown in the *Figure 4.7*. There is an exponential relation between the preconsolidation pressure and the maximum strain (*Figure 4.7*): the more the sample is compacted, the more it tends to swell (positive strains) rather than to collapse (negative strains). This is partially explained in the following paragraph, once the swelling pressure is determined and deeply analysed by the Barcelona Basic Model, presented in *Subsection 5.1.3*.
Under the hypothesis of saturation at the height stabilisation, for the considered sample heights (presented in *Table 4.1*), the saturation phase lasted not more than 2 days.

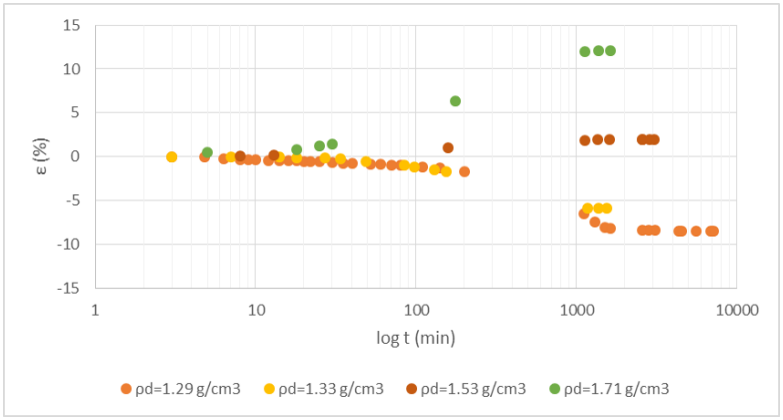

Figure 4.6: *Sample strain evolution with time*

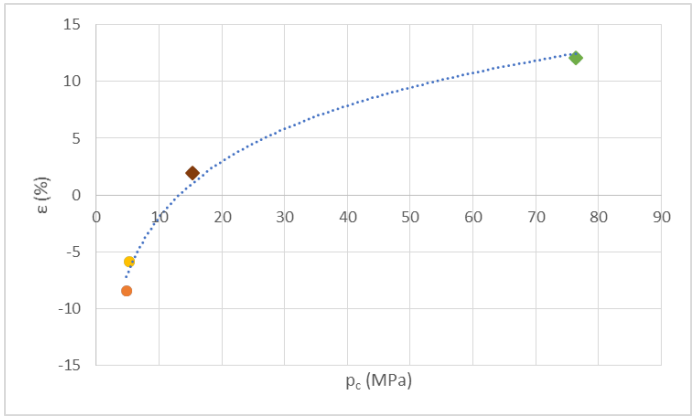

Figure 4.7: *Relation between preconsolidation pressure and maximum strain (swelling or collapse)*

4.3 Hydrated unloading phase

The final step of the swelling test is the unloading phase under saturated conditions: in order to obtain the swelling pressure *Sp*, a series of unloading steps have been applied and the final displacement for each step has been monitored. The aim is to draw a graph *applied pressure vs void ratio difference*, in order to estimate the swelling pressure corresponding to a null void ratio difference. In fact, in oedometric conditions, this means a null deformation (4.2), that is the condition where a swelling pressure develops. The void ratio variation has been calculated from the monitored variation in the sample height, according to the relation:

$$\frac{\Delta V}{V_0} = \frac{\Delta H}{H_0} = \frac{\Delta e}{1 + e_0} \tag{4.2}$$

As previously explained, the sample cannot be considered saturated during the whole phase, because the mechanical swelling due to the unloading generates more void-spaces, and thus the degree of saturation decreases. Since the hydration is allowed, the sample resatures; this coupled phenomenon occurs for each unloading step.

The *Figure 4.8* shows the estimation of the swelling pressure for samples at

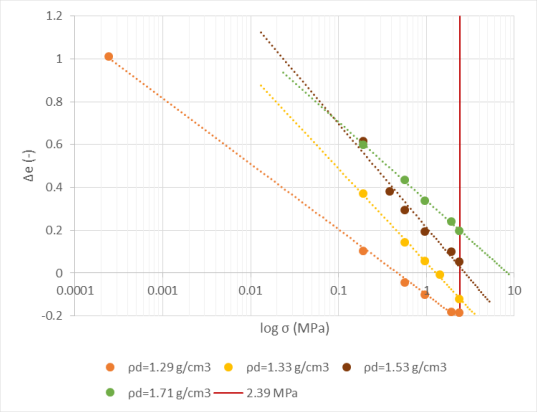

Figure 4.8: *Graphic estimation of the swelling pressure, and comparison with the constant applied pressure (2.39 MPa)*

different initial dry density: there is a clear semi-logarithmic relation between the strains, expressed as void ratio difference Δe, and the applied pressure. For the two samples which shrinked during the hydration phase the swelling pressure has been estimated by the interpolation of the experimental data, whereas for the two samples which have swelled it has been estimated through data extrapolation.

4.4 Discussion

By regarding the *Table 4.2* it can be deduced that, during the hydration phase, the samples with a swelling pressure bigger than the constant applied pressure (2.39 MPa) tend to swell; otherwise, they tend to collapse.

The sample with an initial dry density ρ_d of 1.53 g/cm^3 displays a swelling pressure close to the applied pressure: similarly, this shows a lower height modification. The bigger is the difference between the swelling pressure and 2.39 MPa, the bigger is the modulus of the displacement.
Now, by comparing the swelling pressures to the initial dry densities of the compacted bentonite, the obtained experimental results are in line with the literature (Villar, 2004): the increase of the **initial dry density** rises the swelling pressure of the bentonite exponentially (*Figure 4.9*). The more the bentonite is compacted, the more strongly it vertically swells.

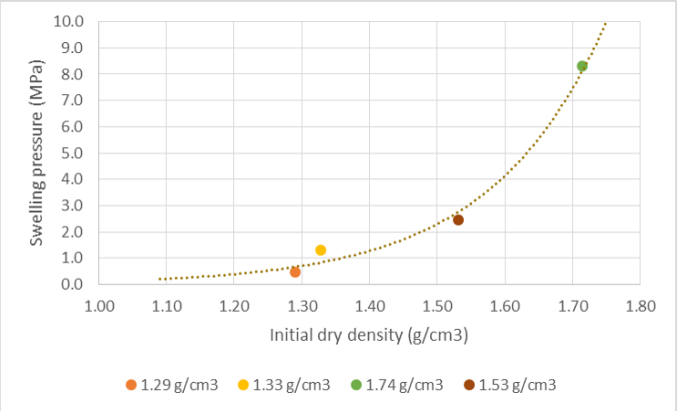

Figure 4.9: *Swelling pressure graphic estimation*

The *Table 4.2* summarizes the obtained results.

Table 4.2: *Comparison of the experimental results*

	Preconsolidation pressure (MPa)	**Initial dry density (g/cm^3)**	**Swelling pressure (MPa)**	**Exhibited Behaviour**
1	4.79	1.29	0.4	Collapse
2	5.23	1.33	1.29	Collapse
3	15.28	1.53	2.47	Slight swelling
4	76.39	1.71	8.33	Swelling

In order to better evaluate the volume change and the variables affecting it, further test are suggested. Since the swelling pressure increases with the smectite content (Villar, 2004), tests on different kinds of bentonite-based materials could be performed. Water with different salinities can be used for the hydration phase, in order to confirm the negligible effect of salinity on high density compacted bentonites (Karnland, 2002). Finally, it is suggested to perform suction-controlled swelling tests, to be able to relate the preconsolidation pressure to the suction: it should increase with suction (Villar, 2004).

Chapter 5

Modelisation

Modelisation is a crucial phase in every geotechnical study, in order to recognize and foresee the soil behaviour: it is an unavoidable simplification of the reality. A constitutive model is deduced from both the theoretical schemes of the continuum mechanics and the results obtained with experimental tests in the laboratory or in-situ (Magnan, 1991): it is the engineer's task to find the most suitable model describing the soil behaviour.
In the current study, it has been decided to model the hydration phase, where the compacted bentonite is saturated under a constant load of 2.39 MPa: the dual behaviour (swelling or collapse) of the samples during this phase could allow to make some comments on the chosen model, and vice versa the model itself, if chosen in an appropriate way, could explain the dual behaviour.
In order to model the hydro-mechanical behaviour of the compacted bentonite, a coupled approach is needed: as regards the mechanical response, different constitutive models have been investigated.

The finite element code **LAGAMINE** has been used. This was developed at the University of Liege (Belgium) at the end of the 1970's, initially for the numerical modelling of large strain, large displacement mechanical problems and contact problems. It takes its name from an anagram of the french word *laminage*, meaning *metal forming*, which is essentially what it was born for.
The code has been further specialised in metal behaviour and, since the 80's, in geomechanics. As regards the latter one, the main research topic is related to environmental geomechanical problems, such as underground nuclear waste storage, geothermal reservoirs, oil and gas reservoirs. For their nature, these need chemo-thermo-hydro-mechanical coupled models.
LAGAMINE is in continuous development thanks to the researcher team working on it; it has been presented in different Belgian and European projects and it finds applications worldwide, in universities as well in the industry, remaining at the leading edge of technology and research.

Problem Under the hypotheses of axisymmetric problem, a bidimensional hydro-mechanical problem has been implemented.

Geometry The modelled sample has a diameter of 50mm: since the problem has been defined as axisymmetric, the numerical analyses have been performed on a rectangle 25 mm large, representing the right unit sector of the cylindrical sample.
The initial height is the height assumed before the hydration phase, different for each test.
Since the sample is laterally confined and the expected strains are only vertical, a finer discretisation is advisable in the vertical direction: the length consists of 10 elements, whereas the height consists of 50 elements, in order to better detect the vertical gradients (*Figure 5.1*). The chosen element has 8 nodes and 4 integration points.

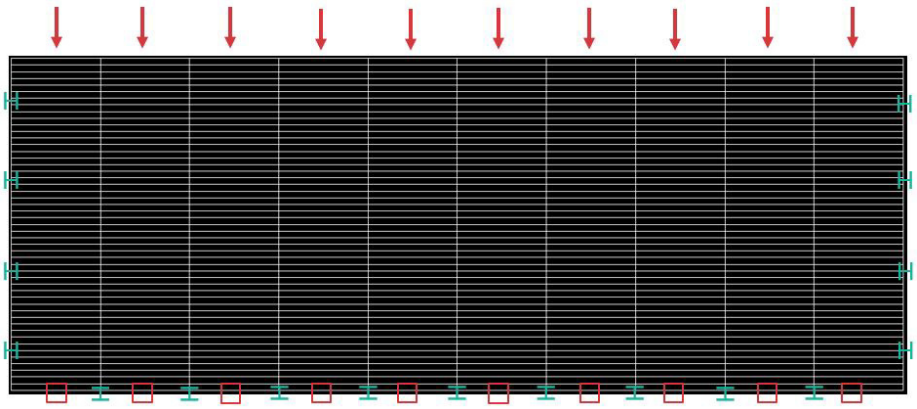

Figure 5.1: *Geometric, boundary (in jade green) and initial (in red) conditions of the analysed problem*

Boundary conditions Due to the problem geometry, the horizontal displacements at the lateral boundaries and the vertical displacement at the bottom of the sample (lower boundary) are supposed to be impeded (jade green signs in *Figure 5.1*). The lateral and upper boundaries are supposed to be waterproof. The water flows vertically from the bottom; the basis, initially having a suction of 53.6 MPa (red squares in *Figure 5.1*), is supposed to be saturated (s=0) after 40 s from the beginning of the hydration phase.

Initial conditions The initial suction equal to 53.6 MPa, assessed through the soil-water retention curve (*Section 3.1*), is applied in all the domain as initial condition.
A constant and uniform pressure of 2.39 MPa is applied on its top for the whole duration of the modelisation; it is represented by the red arrows in *Figure 5.1*.

5.1 Unsaturated soils: governing equations

5.1.1 Effective and total stresses

As the soil includes different status phases, its behaviour has to be studied by establishing an interaction law between the phases themselves. This law takes the name of *effective stress principle*, proposed by Terzaghi (1943).
By considering a completely saturated sample, two stresses acting on it can be identified: the effective stress σ', directly on the grain structure (solid phase), and the neutral pressure u_w, on the water included in the pores (liquid phase). Thus, the effective stress is worked out as the difference of the total stress σ and the neutral pressure:

$$\sigma' = \sigma - u_w \delta \tag{5.1}$$

where δ is the Kronecker delta. On the other hand, when the soil is partially saturated, two state variables describe its behaviour: the net stress $\sigma - u_a$ and the matrix suction $s = u_w - u_a$, where u_a is the air pressure in the pores. Different equations have been proposed to link the two variables; the most common and the one used in this work is the Bishop's equation:

$$\sigma' = (\sigma - u_a) + \chi \zeta s \delta \tag{5.2}$$

where:

χ is the Bishop parameter, depending on the material saturation, and included between 0 and 1; for these reasons, a common simplification is to consider it equal to the degree of saturation;

ζ is the Biot coefficient, equal to $\zeta = 1 - K_b/K_s$; K_b is the drained bulk modulus of the porous solid and K_s is the bulk modulus of the grains; for simplifying reasons it has been assumed equal to 1 in this study.

Thus, under the above-cited simplifications and by assuming the air pressure constant and equal to the atmospheric pressure (u_a=100 kPa), the Bishop's model becomes:

$$\sigma' = (\sigma_{net}) + Sr \cdot s \cdot \delta \tag{5.3}$$

5.1.2 Hydraulic model

The considered hydraulic model is built on the fluid mass conservation principle (5.4) and on the flow governing equation (5.5):

$$\frac{\partial}{\partial t}(\rho_w \cdot \theta) + div(\rho_w \cdot \boldsymbol{q}) = 0 \tag{5.4}$$

$$\boldsymbol{q} = -\frac{K}{\eta}[\boldsymbol{grad}(u_w) + \rho_w \cdot g \cdot \boldsymbol{grad}(z)] \tag{5.5}$$

where:

ρ_w is the water density, equal to 1'000 kg/m^3 and constant since the water is assumed incompressible

θ is the volumetric water content, expressed by the *Equation 3.4*

η is the water dynamic viscosity, equal to 10^{-3} Ns/m^2 in case of water at 20°C

q is the specific discharge (m^3/s/m^2)

K is the intrinsic permeability of the soil (m^2), defined as a function of the relative permeability coefficient (*Equation 3.8*)

u_w is the water pressure (Pa)

g is the gravitational acceleration, equal to 9.81 m/s^2

z is the vertical upward directed coordinate (m)

By assuming a homogeneous material and an isotropic intrinsic permeability K, this can be considered constant in space and time; this is a simplifying hypothesis of the model, since the assumption of isotropy is hard to believe especially in a clay expansive material, where the laminae take a vertical orientation. Moreover, by considering constant values for the water density, the water dynamic viscosity and the gravitational acceleration, and by assuming a vertical water flow (z-direction), the two equations can be rewritten as:

$$\frac{\partial(Sr \cdot n)}{\partial t} = \frac{K}{\eta}\frac{\partial^2(u_w)}{\partial z^2} \tag{5.6}$$

This equation combines the mass conservation principle, allowing the solid frame of the soil to deform itself, with the flow governing equation: it states the dependence of the saturation degree and of the water pressure on both time and space (only vertical direction).

5.1.3 Mechanical models

Drucker-Prager model

The most used constitutive laws in soil mechanics context are elasto-perfectly plastic laws for frictional materials: since the preferable one for soils is the Drucker-Prager model (Magnan, 1991), this has been studied first.

Mathematical formulation The **Drucker-Prager model** has been formulated in 1952 in order to solve a mathematical-kind problem of the Mohr-coulomb model: in fact, the gradient of the plastic function is not defined univocally on the pyramid edges of this latter one; to remedy it, the two scientists proposed to approximate the pyramid with a cone which axis is the trisector of the first octant. By varying the parameters of the model, the cone can inscribe (*Figure 5.2*), circumscribe or approximate the Mohr-Coulomb model in the most suitable way (Nova, 2002). The yielding surface f defined by the Drucker-Prager

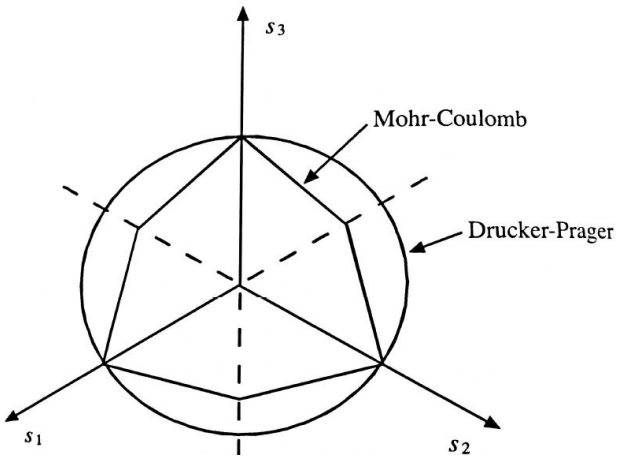

Figure 5.2: *Mohr-Coulomb and Drucker-Prager yielding criteria in the octaedral plane (Nova, 2002)*

criterion is:

$$f = q - Mp' - k = 0 \tag{5.7}$$

where:

q is the deviatoric stress

p' is the mean effective stress

M and k are parameters depending on the soil type.

The plastic strains ε^{pl} are worked out through the *non-associated flow rule* implemented by the code:

$$\dot{\varepsilon}^{pl} = \dot{\lambda}\frac{\partial G(\boldsymbol{\sigma})}{\partial \boldsymbol{\sigma}} \tag{5.8}$$

where:

λ is a non-negative scalar parameter

$G(\boldsymbol{\sigma})$ is the plastic potential

$\boldsymbol{\sigma}$ is the stress matrix.

Since the flow rule is non-associated, the plastic potential does not coincide with the yielding surface; however, it has a similar equation:

$$G(\boldsymbol{\sigma}) = q - M^* p' - k^* = 0 \tag{5.9}$$

The parameters M, M^*, p and p^* are defined as: where:

Table 5.1: *Yielding surface and plastic potential parameters*

Yielding surface f	**Plastic potential $G(\sigma)$**
$M = \frac{6sin\varphi'}{3 - sen\varphi'}$	$M^* = \frac{6sin\varphi'}{3 - sen\varphi'}$
$k = \frac{6c'cos\varphi'}{3 - sen\varphi'}$	$k^* = \frac{6c^*cos\psi}{3 - sen\psi}$

φ' is the drained friction angle

c' is the drained cohesion

ψ is the dilatation angle

c^* is a coefficient, different from the cohesion c'.

Moreover, the Drucker-Prager model represents an extension of the Von Mises criterion, as shown in *Figure 5.3* (Nova, 2002): whereas hydrostatic pressure independence is a realistic assumption for metals, soils do not show symmetrical behaviour under positive (compressive) and negative (tensile) stresses, so the Von Mises criterion is not suitable for them; thus, the cylinder infinitely extended in three dimensional principal stress space hypothesized by Von Mises becomes a cone in positive stresses in the Drucker-Prager model, where the shear strength increases with the isotropic pressure.

Mechanical parameters determination

Cohesion c' and friction angle $\boldsymbol{\varphi'}$ The two parameters M and k both depend on the drained friction angle $\boldsymbol{\varphi'}$ and the drained cohesion $\boldsymbol{c'}$. Since the cohesion and the friction angle can be experimentally determined from shear tests, not performed in the context of this study, data from literature have been used.

The cohesion value of inorganic compacted clay of high plasticity, as the bentonite in this study, varies from 11 kPa to 103 kPa, and decreases as the saturation degree increases (NAVFAC, 1986); since the model considers a constant value of cohesion, a mean value has been chosen equal to **60 kPa**. The frictional angle has been chosen equal to **19**° (Carter, 1991).

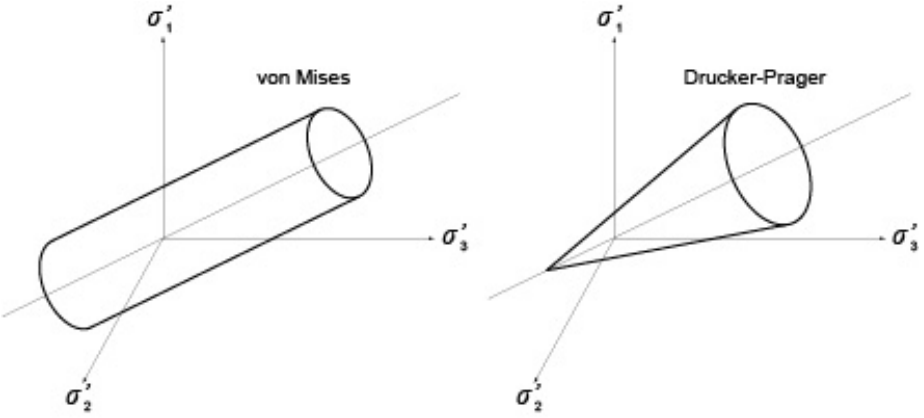

Figure 5.3: *Yield surfaces for the Von Mises (left) and Drucker-Prager (right) constitutive models (Taborda, 2012)*

Stiffness parameters The Young elastic modulus E and the Poisson ratio ν define the stiffness matrix D and thus the elastic component of the strains; under the hypothesis of isotropic material, the linear elastic behaviour is finally determined by these two parameters.
Whereas for the Poisson ratio $\boldsymbol{\nu}$ a value equal to **0.3** has been chosen from Gerard et al. (2008), the Young modulus **E** has been experimentally estimated. Since the soil does not behave linearly, but its stiffness increases with the sample compaction, the Young modulus has been worked out by the oedometric modulus E_{Ed} through the (5.10):

$$E = E_{Ed}\frac{(1+\nu)\cdot(1-2\nu)}{1-\nu} \tag{5.10}$$

where the oedometric modulus has been assessed as $E_{Ed} = \dfrac{\Delta}{\sigma}\Delta\varepsilon$ by the *Figure 5.4*. This represents the compaction phase of three different samples initially in powder state; in order to reach wider range of preconsolidation pressure, the compaction has been made at the press. Usually, the oedometric modulus has calculated through the unloading phase, where the soil has a linear behaviour. By regarding the unloading phase, it is possible to deduce a very great oedometric value and thus a very great Young modulus: this is due to a non-negligible effect of the friction between the sample and the ring wall. Thus, it has been decided to estimate the oedometric modulus through a loading step, arbitrarily established. By choosing an opportune loading step (12 MPa-27 MPa, represented by darker tracts in the *Figure 5.4*), a Young modulus of 152.36 MPa has been estimated, in agreement with what found by Gerard et al. (2008).

Comparison with the experimental results By regarding the yield curve in the *p'-q* plane (*Figure 5.5*), the sample reaches the plastic domain at the end of the test: this could explain the height stabilisation of the samples during the experimental tests.
Since the relationship stresses σ - strains ε can be expressed by the incremental relation (in a matricial way $\dot{\boldsymbol{\sigma}}' = \boldsymbol{D}\dot{\boldsymbol{\varepsilon}}$), in the elastic domain the strains increase

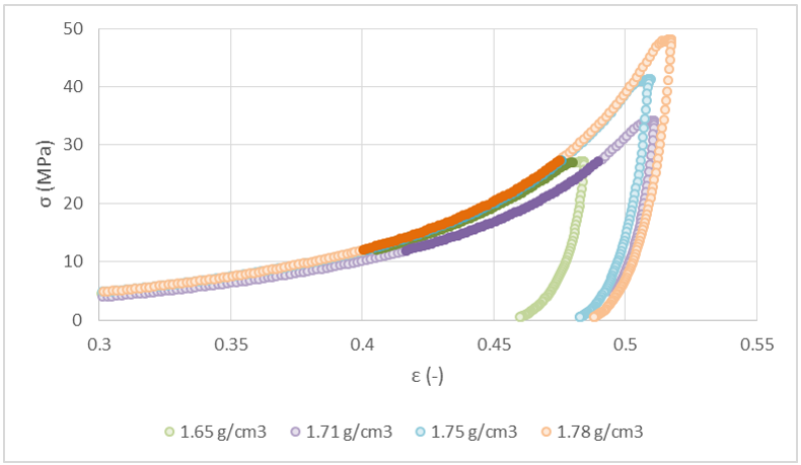

Figure 5.4: *Experimental determination of the oedometric modulus* E_{Ed}

Table 5.2: *Needed parameters for the Drucker-Prager model*

	Experimentally determinated	**Model calibration**	**Datum from literature**
c' (kPa)			60
$\boldsymbol{\varphi'}$ (°)			19
$\boldsymbol{\nu}$ (-)			0.3
E (MPa)	152.36		

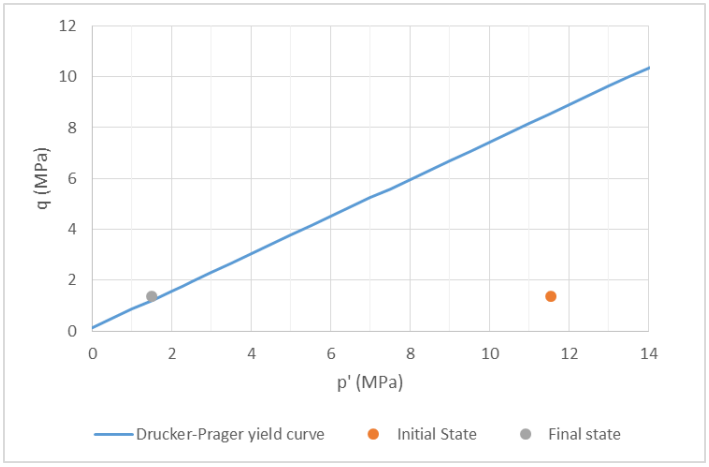

Figure 5.5: *Drucker-Prager model in p'-q space*

(or decrease) with the effective stress.
Both the initial and the final effective stresses can be calculated by the Bishop's equation (5.3):

the total stress σ is the applied load, equal to 2.39 MPa and constant during the hydration phase;

the initial degree of saturation is calculated as $Sr = \frac{\rho_s \cdot w}{\rho_w \cdot e} = 0.30$, the final one is assumed equal to 1;

the suction is assessed from the soil-water retention curve (*Section 3.1*), starting from the saturation degree value.

After calculating the effective stress values for the initial and the final states (*Table 5.3*), it is possible to deduce that the Drucker-Prager model provides a swelling behaviour of the sample. In fact, a decrease in effective stress means a decrease in strains too.

Table 5.3: *Initial and final state of the sample, during the hydration phase*

	Initial state	**Final state**
Total stress σ (MPa)	2.41	2.41
Saturation degree Sr (-)	0.30	1
Suction s (MPa)	53.6	0
Effective stress σ' (MPa)	18.63	2.41
p' (MPa)	11.5	1.49
q (MPa)	1.38	1.38

Figure 5.6 shows the swelling behaviour foreseen by the model: it well reproduces one of the three samples behaviour for the first 100 minutes, but after 100 minutes it overestimates the swelling response.

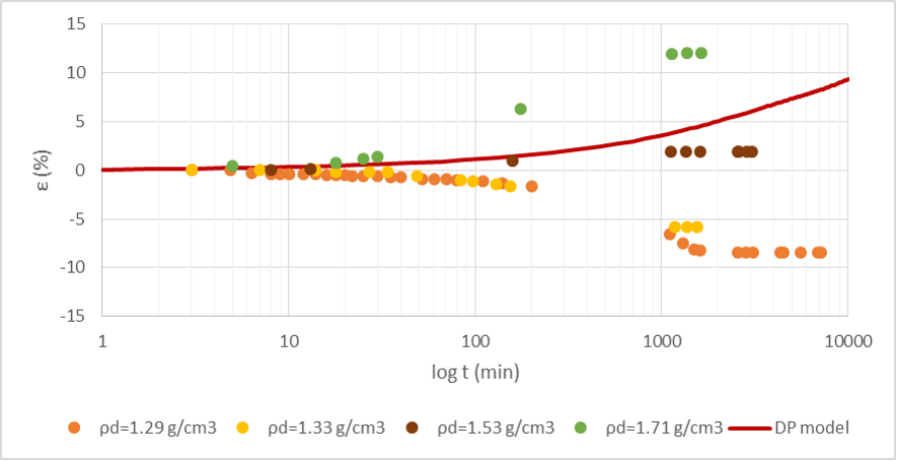

Figure 5.6: *Comparison between the experimental data and model*

Moreover, since the samples show different behaviours (swelling or collapse) depending on the preconsolidation pressure, and the Drucker-Prager model does not consider it, this criterion cannot explain the dual behaviour experimentally observed; for which reason further models have been investigated.

Modified Cam-Clay model

In porous materials, such as compacted bentonite, a large part of the volume consists of voids which may be filled by fluids, both air and water. As a result, deformations in soil are accompanied by large and mostly irreversible volume changes (Nova, 2002). Thus, the **Modified Cam-Clay model** has been applied, since it has been developed especially for clay materials, as its name suggests.
Thus criterion is able to consider the irreversible strains occurring even far from the breakage and to take into account the preconsolidation pressure (crucial in determining if the sample swells or collapses during the hydration phase).

Mathematical formulation

The Cam-Clay model implies a hardening elasto-plastic constitutive law, which means yielding increasing with the plastic strains (Nova, 2002). Permanent strains develop only when the clay is normal-consolidated, whereas elastic strains develop under over-consolidation conditions. This behaviour can be explained by considering *Figure 5.7*, where the virgin consolidation line and a swelling line are represented. The specific volume v depends on the void index e by the following relation:

$$v = 1 + e \tag{5.11}$$

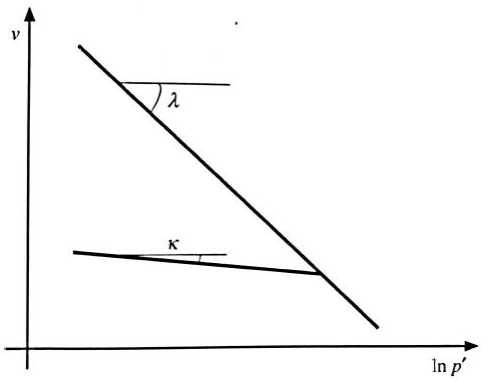

Figure 5.7: *Relation between the specific volume and the mean pressure, according to the Cam-Clay model (Nova, 2002)*

By loading the sample with an effective vertical pressure p' greater than the preconsolidation pressure p_c', the sample develops plastic strains and the image point moves along the **virgin consolidation line** whit a λ-slope: the soil is normal-consolidated. Then, by unloading and reloading the sample up to a pressure lower than the maximum one experienced by the soil, it moves along a **swelling line**, characterized by a κ-slope. Whereas the virgin consolidation line is unique for one test, the swelling lines can be multiple, depending on the unloading-reloading pressures.

Another important concept in the modified Cam-Clay model definition is the **critical state**. It is defined by:

a constant pressure ratio $\frac{q}{p} = M$;

no volume change;

and it is represented by:

a straight line parallel to the virgin consolidation line in the *v-lnp'* plane;

a straight line passing through the origin, with M-slope, in the *q-p'* plane (*Figure 5.9*).

The modified Cam-Clay model is defined in term of deviatoric stress q and mean effective stress p' as:

$$\frac{q_2}{p'^2} + M^2\Big(1 - \frac{p'_c}{p'}\Big) = 0 \tag{5.12}$$

where M is a model parameter calculated as in the Drucker-Prager model.

Parameters determination

Cohesion c' and friction angle φ' As regards the cohesion, the friction angle and thus the parameter M, they are the same used in the Drucker-Prager model.

Stiffness parameters Both the stiffness parameter λ and the elastic stiffness parameter κ, respectively defining the virgin consolidation line and the swelling lines in the *lnp'-v* plane, have been experimentally assessed from the compaction phase of different samples. *Figure 5.8* shows a good reliability of the estimated values: even if the maximum pressure is different, the samples display very similar behaviours and very similar slopes too. The different dry densities reached are shown.
The normal-consolidation coefficient λ has been determined by looking at the linear part of the virgin curve; the over-consolidation coefficient κ has been determined as the slope of the unloading-reloading curve. The estimated value are presented in *Table 5.4*.

Table 5.4: *Plastic parameters for the modified Cam-Clay model*

	Experimentally determinated	**Model calibration**	**Datum from literature**
$\boldsymbol{\lambda}$	0.695		
$\boldsymbol{\kappa}$	0.074		
c' (kPa)			60
$\boldsymbol{\varphi'}$ (°)			19
$\boldsymbol{\nu}$ (-)			0.3

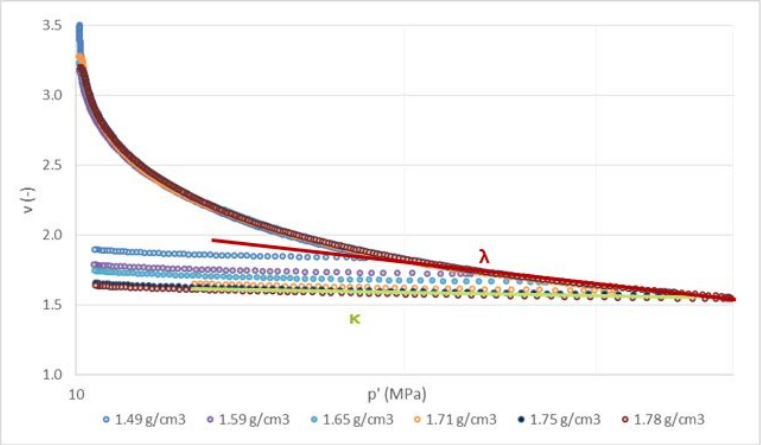

Figure 5.8: *Experimental determination of the model parameters*

Comparison with the experimental results The modified Cam-Clay criterion (*Equation 5.12*) plots as an elliptical curve in the *p'-q* plane, with two vertices laying on the x-axis: one on the origin and one on a point corresponding to the preconsolidation pressure p_c'; the critical state line intersects the yield surface at the point of maximum q value.

Initial and final stress states are calculated as in the *Subsection 5.1.3*.

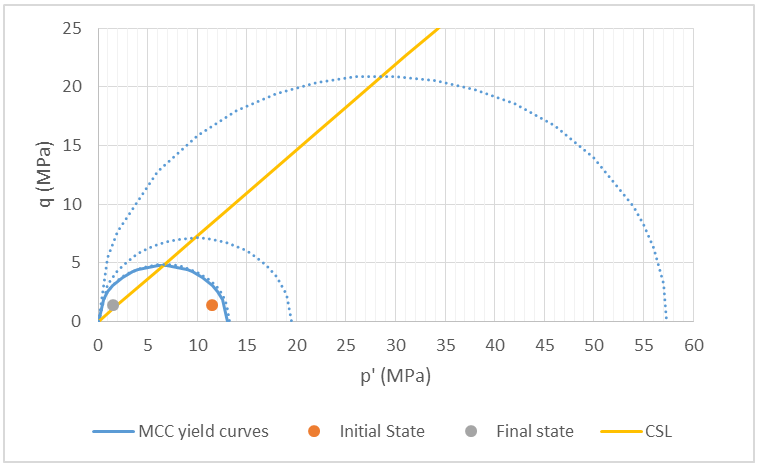

Figure 5.9: *Modified Cam-Clay model in p'-q space*

As regards the initial state, since the model reproduces the porous soil behaviour, also the initial porosity n_0 (before the wetting path) has to be estimated. It can be easily determined from its definition:

$$n = \frac{V_v}{V} = \frac{V - V_s}{V} = 1 - \frac{M}{(w+1)\rho_s V} \tag{5.13}$$

Since the mass M has been weighed, the total volume V is known thanks to the measured height displacement and the fixed diameter, and the initial water

content has been calculated, the assessed initial porosity is equal to 0.53.
Figure 5.9 presents the experienced path and the yield curves for different preconsolidation pressures: for greater preconsolidation pressures, the yield surfaces extend towards right, but both initial and final states remains included in them. Therefore, the modified Cam-Clay model provides an elastic behaviour for the samples, during the whole test. For what discussed before, the expected modelled behaviour is only swelling trend: in fact, negative strain difference occurs for negative stress difference ($\dot{\boldsymbol{\sigma}}' = \boldsymbol{D}\dot{\boldsymbol{\varepsilon}}$). By regarding *Figure 5.10*, it is possible

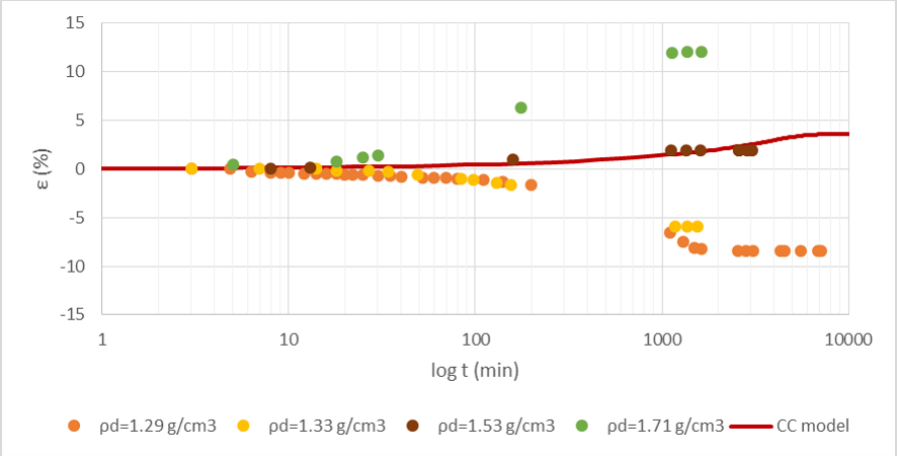

Figure 5.10: *Comparison between the experimental data and model*

to observe a final stabilisation of the height, that is a more realistic behaviour than the one of Drucker-Prager criterion. Although the modified Cam-Clay model considers the preconsolidation pressure in its mathematical formulation, it does not affect the response of the modelled sample, because both the initial and final states are included in all the yield surfaces (*Figure 5.9*).

Barcelona Basic Model

Both constitutive models applied so far are unable to reproduce the behaviour of the bentonite sample during the hydration phase: neither considers the suction in its implementation, relevant parameter especially for partially saturated soils. Now, the **Barcelona Basic Model** is applied, since it describes the stress-strain behaviour of partially saturated soils; it can represent also some features of the behaviour of expansive clays, such as compacted bentonite. It has been formulated within the framework of hardening plasticity using two independent sets of stress variables: the excess of mean stress over air pressure (or net mean pressure) p_{net} and the suction s (Alonso, 1990). Once saturation is reached, the model acts as a conventional critical state model.

Mathematical formulation Suction plays a fundamental role in the partially saturated soils behaviour: experimental tests illustrated by Alonso et al. (1990) highlight a soil stiffening and strengthening when suction increases. In turn, this produces a decrease in compressibility, an increase in the shear strength and in the apparent preconsolidation pressure.
Moreover, a reduction in suction during a wetting path, under a given confining stress, may induce an irrecoverable volumetric compression, due to the pore collapse.
This latter evidence and the increase in apparent preconsolidation pressure shape the **LC yield curve** (after loading-collapse) in the p_{net}-s plane. This limits the elastic domain, within it the soil is over-consolidated and the strains are reversible (*Figure 5.11*).
From a mathematical point of view, the LC curve is worked out as:

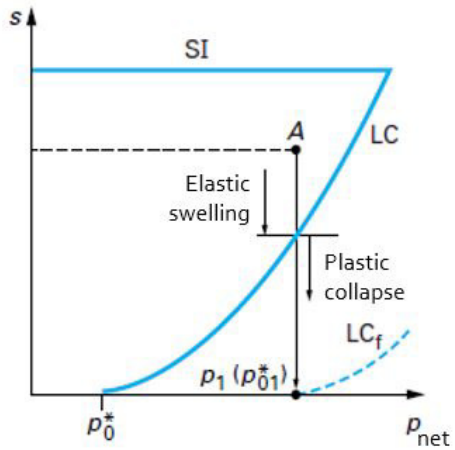

Figure 5.11: *Loading-collapse (LC) and suction increase (SI) yield curves; wetting path represented by the Barcelona Basic Model (picture modified from Delage, 2015)*

$$\left(\frac{p_0}{p^c}\right) = \left(\frac{p_0^*}{p^c}\right)^{\frac{\lambda(0)-\kappa}{\lambda(s)-\kappa}} \tag{5.14}$$

where:

p_0 is the net preconsolidation stress, calculated for different suctions;

p^c is the reference pressure, assumed equal to the atmospheric pressure p_{atm}=100 kPa;

p_0^* is the net preconsolidation stress for saturated conditions, laying on the x-axis (s=0);

λ_0 is the stiffness parameter for saturated conditions;

λ_s is the stiffness parameter for changes in net mean stress for virgin states of the soil, function of the suction;

κ is the elastic stiffness parameter for changes in net mean stress.

In turn, the stiffness parameter λ_s can be calculated as a function of the suction s; different equations are available to this purpose. In this study the following one has been adopted, given that it predicts an asymptotic maximum stiffness:

$$\lambda_s = \lambda_0[(1-r)exp(-\beta s) + r] \tag{5.15}$$

where:

r is a constant related to the maximum stiffness of the soil for an infinite suction, $r = \dfrac{\lambda(s \to \infty)}{\lambda(0)}$;

β is a parameter controlling the rate of increase of soil stiffness with suction.

Figure 5.11 also schematizes the wetting path followed by the samples during the hydration phase. It highlights two different behaviours: a swelling trend within the elastic domain and a collapsing trend when the soil is plasticized.
The preconsolidation pressure makes the LC curve shift towards right, and given that the initial and the final states are the same for each sample, the more the preconsolidation pressure increases, the more the sample remains in the elastic domain (*i.e.* swells). This could explain the dual behaviour, swelling or collapsing, of the samples during the hydration phase, already outlined in *Section 4.2.*

As stated before, an increase in suction may also induce irreversible strains: it means that the elastic domain limited by the LC curve cannot extend indefinitely for high suction values. The model provides an **SI yield curve** (after suction increase), corresponding to the maximum previously attained value of suction (Alonso, 1990). This is represented by a straight line in the p_{net}-s plane (*Figure 5.11*).
Adopting a linear dependence between the specific volume v and the logarithm of the suction *lns* (*Figure 5.12*), both in the elasto-plastic and in the elastic domain, one may write, for virgin states:

$$dv = -\lambda_s \frac{ds}{(s + p_{atm})} \tag{5.16}$$

where λ_s is the stiffness parameter for changes in suction for virgin states of the soil (Alonso, 1990). Similarly, for drying and wetting paths under lower suctions:

$$dv = -\kappa_s \frac{ds}{(s + p_{atm})} \tag{5.17}$$

In this study, the maximum experienced suction has been assumed very high, in order to not perturb the applied suctions range.

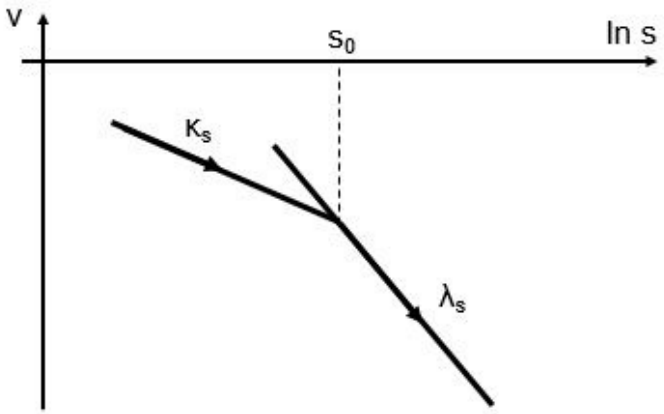

Figure 5.12: *Definition of yield suction s_0*

As regards the initial porosity, the same comments as in *Subsection 5.1.3* can be made.

Parameters

Experimental determination It is possible to assume a constant value of $\boldsymbol{\kappa}$, independent on the applied suction (*Figure 5.14*). It can be experimentally determined from the compaction phase, as for the modified Cam-Clay model: the elastic stiffness parameter is the slope of the unloading phase, in p_{net}-v plane. Since the reference system is different between the modified Cam-Clay and the Barcelona Basic models, also the assessed value is different. *Figure 5.15* shows similar κ coefficients for different samples: the estimated value is equal to **0.021**. It is in agreement with the value proposed by Alonso et al. (1990). Since the maximum experienced suction s_0 has been assumed very high, the stiffness parameter λ_s cannot be experimentally determined. On the other hand, by reproducing the *Figure 5.12* with the experimental data, the elastic slope $\boldsymbol{\kappa_s}$ can be assessed. Data from the soil-water retention curve have been considered: under unconfined conditions, they have experienced different suctions s and shown different specific volumes v (*Figure 5.16*). The estimated κ_s is equal to **0.114**.

Model calibration The model parameters r and β, together with the preconsolidation stress for saturated conditions p_0^*, have been estimated through a model calibration, by imposing that the point ($\mathrm{p_c}$; $\mathrm{s_i}$), corresponding to the

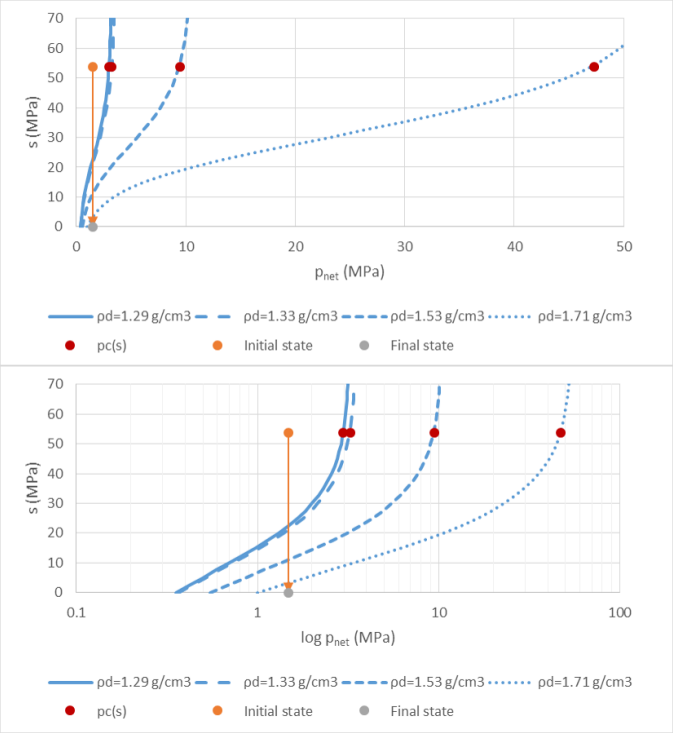

Figure 5.13: *Yield curves after the model calibration*

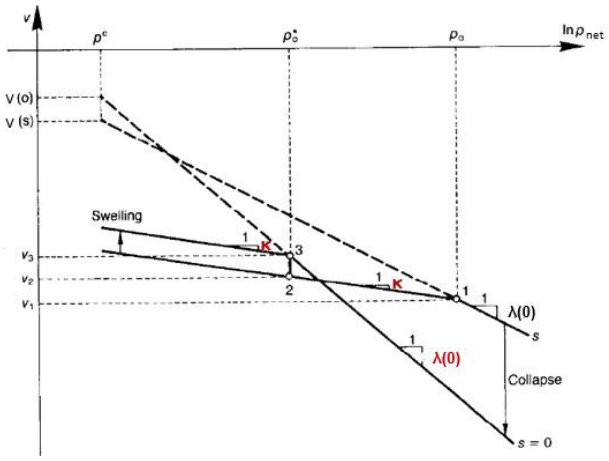

Figure 5.14: *Compression curve for saturated and unsaturated soils (modified from Alonso, 1990)*

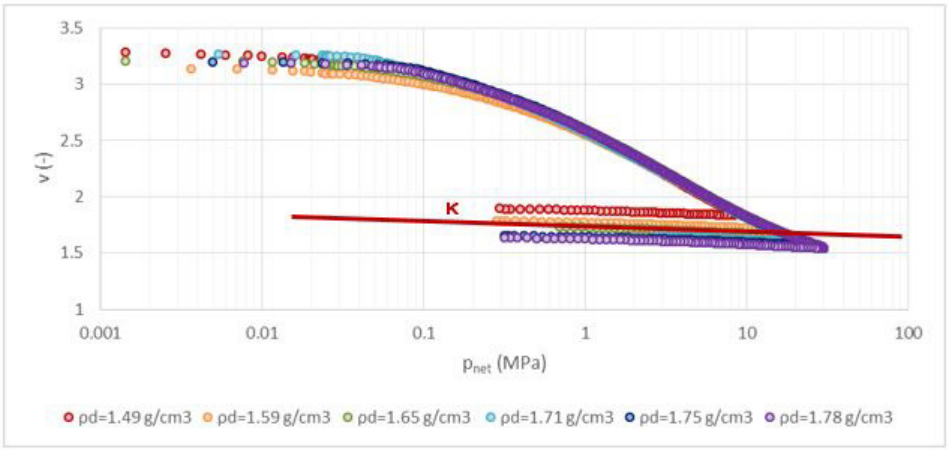

Figure 5.15: *Experimental determination of* κ

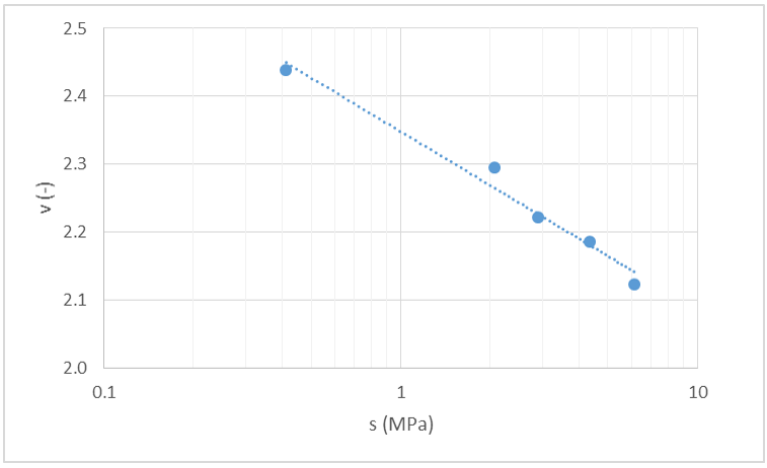

Figure 5.16: *Experimental determination of* κ_s

preconsolidation pressure at the initial suction, lays on the LC curve. This requirement is satisfied for $\boldsymbol{r = 0.4}$ and $\boldsymbol{\beta = 5 \cdot 10^{-2} MPa^{-1}}$. By changing the preconsolidation pressure, only p_0^* changes, while the model parameters remain constant.

Literature For the Poisson's ratio a value equal to 0.3 has been considered (Gerard, 2008).
As regards the stiffness parameter λ_0 in saturated conditions, it was supposed to be calculated by loading a saturated sample beyond its preconsolidation stress p_0^*. Unfortunately, because of a physical limit of the oedometer (maximum load equal to 5.81 MPa), it has not been possible to experimentally determine it. Thus, the value estimated by Dieudonné (2016) in a similar study on compacted bentonite has been used, $\boldsymbol{\lambda_0 = 0.38}$.

Table 5.5: *Parameters for the Barcelona Basic model*

	Experimentally determinated	**Model calibration**	**Datum from literature**
$\boldsymbol{\kappa}$	0.021		
$\boldsymbol{\kappa_s}$	0.114		
$\boldsymbol{r}$		0.4	
$\boldsymbol{\beta}$ (MPa^{-1})		0.05	
$\boldsymbol{\varphi'}$ (°)			19
$\boldsymbol{\nu}$ (-)			0.3
$\boldsymbol{\lambda(0)}$			0.38

Comparison with the experimental results

The initial and final states have been calculated as for the other models, but in terms of net mean pressure, $p_{net} = p - p_{atm}$.
The initial suction has been assessed from the water retention curve, and the final one assumed zero-value.
Table 5.6 summarizes the initial and final states, also shown in *Figure 5.13*. The orange arrow represents the wetting path experienced by the samples; the LC curve shape changes for different preconsolidation pressures at a given suction $p_c(s)$. Depending on it, the samples path in the elastic or in the plastic domain changes: this is better inferable from the semi-logarithmic graph: the more the samples remains in the elastic domain, the more it swells. The *Figure 5.13* also explains the similar behaviour of the two less compacted samples: they have similar LC curves.

By comparing the *Figure 5.13* and *5.17* it is possible to observe that the more the sample persists in the elastic domain, the more it swells; the more the sample experiences the plastic domain, the more it collapses.

From a qualitative point of view, *Figure 5.17* shows more similarities between the model and the reality, rather than those ones obtained by the previous models: the Barcelona Basic model is able to model the dual behaviour of the

Table 5.6: *Initial and final state of the sample, during the hydration phase*

	Initial state	**Final state**
Net mean pressure p_{net} (MPa)	1.49	1.49
Suction s (MPa)	53.6	0

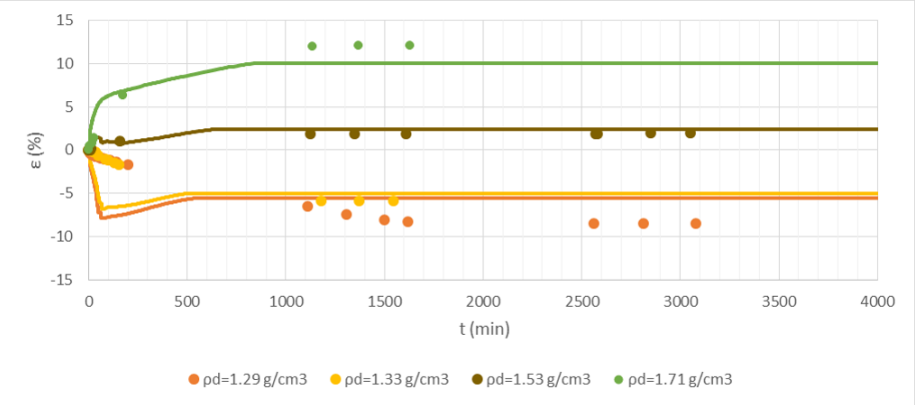

Figure 5.17: *Comparison between the experimental data and model, for different intrinsic permeabilities K*

compacted samples according to the different preconsolidation pressures, and it also represents a similar final strain; in the transient period, it is not able to well represent the observed behaviour for the less compacted samples.
By varying the permeability value, the best compromise is reached for $K = 9 \cdot 10^{-19}$ m^2, close to that one obtained by the consolidation test. It fits well for the two most compacted samples, but it shows a sudden collapse for the two less compacted ones, different from what observed experimentally: this trend is also explained by the *Figure 5.19a*. The modelled porosity suddenly decreases (1 hour) and then increases (1 day): this is because the suction of the two samples decreases suddenly, given that permeability value; thus they immediately experience the plastic domain. Upon hydration, their laminae swell, the porosity increases, the suction decreases, and they come back to the elastic domain and swell. Later, given the continuous hydration, they get saturated and their height reaches a constant value. However, a similar final strain has been obtained.
A better approximation for the two less compacted samples could be reached by assuming a lower permeability: in fact, by collapsing, the porosity strongly decreases and thus also the relative permeability. Since the intrinsic permeability is an intrinsic (and thus constant) property for a given material, some comments could be made about the relative permeability; in this study it has been used the common assumption:

$$k_{rw} = Sr^3 \tag{5.18}$$

Thus, the relative permeability does not consider directly the porosity of the sample. More precise relations between the relative permeability, the degree of saturation and the porosity of the sample are studied by Romero et al. (1999). An improved relation could allow a direct increase of the relative permeability

with the porosity.

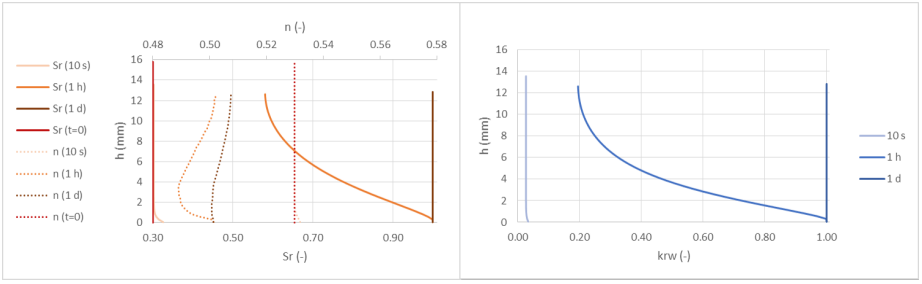

(a) Dry density ρ_d=1.29 g/cm^3

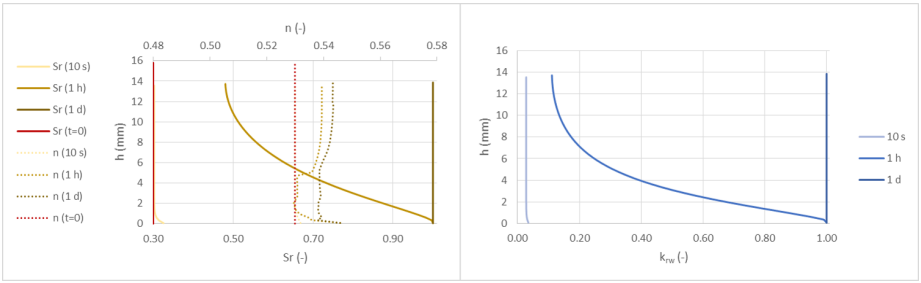

(b) Dry density ρ_d=1.53 g/cm^3

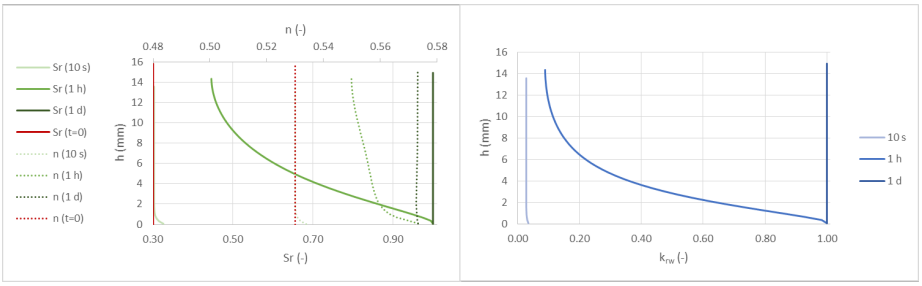

(c) Dry density ρ_d=1.71 g/cm^3

Figure 5.18: *Evolution of saturation degree, porosity and relative permeability for different dry densities*

This limiting aspect of the model is shown in *Figure 5.18*: the relative permeability k_{rw} does not depend on the porosity n, but it perfectly follows the trend of the saturation degree Sr. Since the properties are similar for the samples with similar dry density values (1.29 and 1.33 g/cm^3), only the first one has been represented, in order to avoid a data redundancy. In every case, the modelled permeability increases over time, because the sample progressively saturates. On the other hand, the porosity does not present an univocal trend, as shown also in *Figure 5.19* for different times. By hydrating from the basis, the porosity decreases where the sample is hydrated (collapse): this is because the hydration produces a decrease in suction; thus the hydrated part plasticises first. The more the sample is compacted, the less evident is this dual trend: for the most compacted sample (ρ_d=1.71 g/cm^3), since it becomes plastic only for very low suction (see *Figure 5.13*), each part of the sample swells and its

porosity only increases over time. For the sample compacted at ρ_d=1.53 g/cm^3 the porosity includes a little range of values: in fact, this is the sample with the lowest strain values.

However, the degree of saturation depends on the porosity from the *Equation 5.6*; this relation is inferable from the *Figure 5.19*, especially for times bigger than 1 day. The degree of saturation decreases for higher dry densities: the sample swells strongly, the void spaces increase and thus the saturation degree decreases. On the other hand, the increase in void spaces produces an easier preferential path for the water flow, meaning a higher relative permeability and a greater water volume (i.e. a greater saturation degree). This coupled mechanism makes hard to establish a relation between relative permeability, saturation degree and porosity.

Discussion

By comparing the three applied models, some basic differences have been observed: whereas both the Drucker-Prager and the Cam-clay models do not show any difference in the behaviour of the bentonite compacted at different densities, the Barcelona Basic model can do it and it can also model the pore collapse mechanism, typical of partially saturated soils. Suction is a fundamental quantity acting in unsaturated soil: the Barcelona Basic model is the only one considering it. The plasticization occurs as the suction increases. Thus, this one can be considered the best representative model so far, although the relative permeability is not perfectly represented: a further study about it could be made, deepening the inter-relation between saturation degree, relative permeability and porosity. In order to investigate the dependency of the relative permeability on the porosity, some tests on samples at constant porosity should be made (Romero, 1999). Maintain a constant porosity means do not observe neither swelling nor collapse, that is find a constant load to apply, neither too small causing swelling, nor too big causing collapse: the research of an alike pressure is not easy.
By comparing the degree of saturation at the end of the hydration phase estimated by the three models, the Cam-Clay and the Barcelona Basic models respect the assumption of saturated sample. This is due to a height (and so volume) stabilisation, meaning constant porosity: the more the water flows in, the more the sample saturates. On the other hand, the Drucker-Prager model foresees a bigger height increase, and thus a porosity increase: the saturation degree increases with the flowing water increase, but at the same time it tends to decreases as the void volume increases (Equation 3.3).

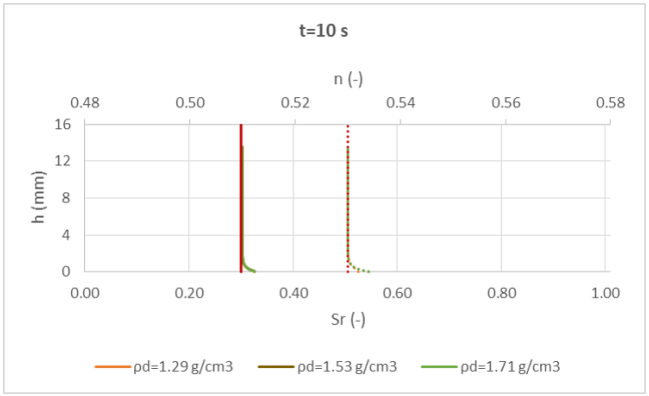

(a)

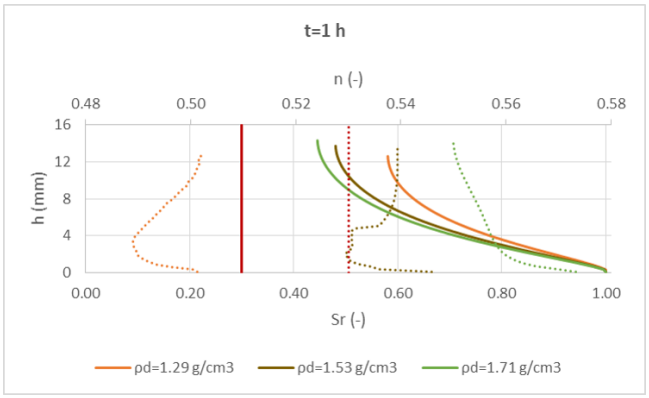

(b)

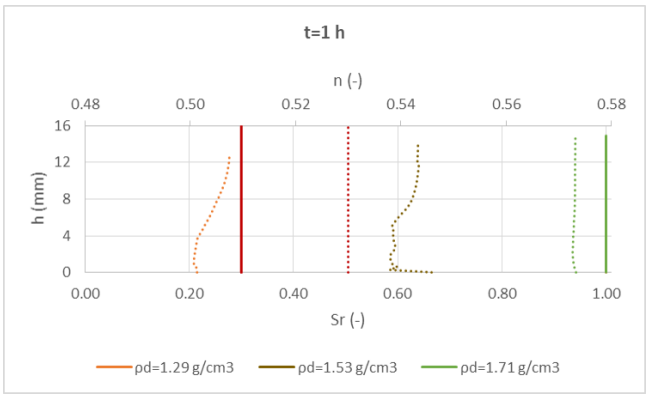

(c)

Figure 5.19: *Saturation degree and porosity for different dry densities and times*

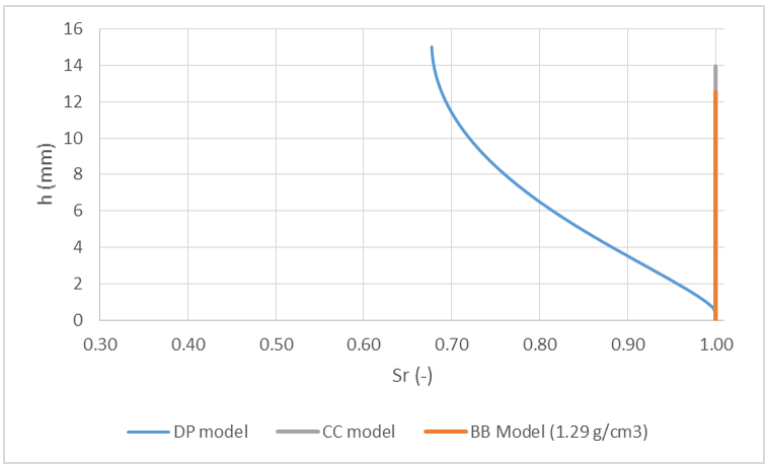

Figure 5.20: *Comparison of the saturation degree obtained by the three models at the end of the hydration phase (12 days)*

Chapter 6

Conclusions

A first aim of this work was to characterise the given bentonite and to compare it with known types, commercialised and already studied.
After comparing the results obtained from the performed experimental tests, it is possible to assert that the results are reliable and physically acceptable, except for the particle density value, generally difficult to estimate. As regards the other results, they are in agreement with the typical parameters assessed for compacted bentonite, and in particular they follow quite well the mineralogical, granulometric and plastic properties of the MX-80 bentonite: this is a world-wide known material implemented as backfilling and sealing body in disposal concepts (Villar, 2004).

Also the hydraulic tests, investigating the soil-water retention curve parameters and the permeability value, have shown results in agreement with the literature data. Some comparisons have been made between the studied bentonite hydraulic behaviour and the mixture of Wyoming MX-80 bentonite and quartz sand used by Gatabin et al. (2016) in its study: they are qualitatively and quantitatively in agreement; this contributes to consider the obtained results as reliable and definite. Moreover, as already accepted by the scientific community for the assessment of the permeability, the greater reliability of a consolidation test rather than a falling head test was proved.

A swelling test has been performed to highlight the most relevant mechanical property of high density compacted bentonite, that is the volume change under hydration. It has produced good and reliable results as much as it has revealed some limitations of the used devices.
First of all, given the high expansive capacity of the compacted saturated bentonite, the oedometric ring should be higher in order to be able to contain the swelled soil without creating any discontinuity in the system: in the used oedometric cell, most of the times the swelled soil came out from the ring, into the discontinuity between the ring itself and the oedometric body. Thus, above the ring, the diameter was greater and the bentonite was allowed to swell not only vertically but also laterally. On the other hand, the used ring satisfied to

the limit requirement for reducing the friction effects ($2.5 < \frac{D}{h} < 6$). By increasing the ring height, this requirement is not satisfied anymore. So, it would be interesting to evaluate which condition is more important to achieve, if a little lateral swelling and negligible friction on the oedometric ring wall, or a prevented lateral swelling with a greater friction. Some tests would be requested to answer this issue.
Moreover, the maximum pressure bearable by the oedometer was a limiting factor: it was very low, in relation to the needed pressures. In fact, the more the bentonite is compacted (*i.e.* the bigger is the preconsolidation pressure), the more it swells. In order to solve this inconvenience, some samples have been compacted by the compacting press. This in turn produces another inconvenience, because the sample has to be moved from the press ring to the oedometric ring, since the further phases of the swelling test (hydration and unloading phases) had to be performed at the oedometer: the repositioning necessarily produces a worse adherence between the soil and the oedometric ring and so the uncontrolled interference of initial lateral swelling. In samples directly compacted at the oedometer, this problem does not occur and the adherence is improved, the initial lateral swelling negligible.
Then, if the odoemeter had born greater pressures, also the stiffness parameter for saturated conditions $\lambda(0)$ would have been estimated: once the compacted samples are saturated and a steady state is reached, pressures of the same order of magnitude of the preconsolidation pressure and higher have to be applied in increasing order. In fact, by unloading the sample, it risks to desaturates because of the combined effect of mechanical unloading and facilitated swelling due to a greater water inflow.
By performing a shear test and a triaxial test, also the cohesion, the friction angle and the Poisson coefficient would have been experimentally determined.

The last aim of the work was to calibrate a model, suitable for predicting with sufficient accuracy the compacted bentonite behaviour. Different models, usually applied on the soil behaviour, have been analysed and between them the Barcelona Basic model seems to be the most suitable. Actually, it has been developed precisely for partially saturated soils, such as hydrated compacted bentonite. The parameters calibration has been made on the hydration phase, since this one has shown the most characterising dual behaviour of the samples: swelling in some cases, collapse in others. From a qualitative point of view, the calibrated model reproduces quite well the soil behaviour. It does not fit very well the transient phase for the less compacted sample: whereas in the reality they collapse in a gradual way, the modelled samples collapse suddenly at the beginning, and then they swell and reach a constant height. A lower permeability could reproduce a behaviour more similar to the observed one, but this would cause a lower swelling in the most compacted samples. A further application could be to improve the relation between the porosity, the saturation degree and the relative permeability, in order to find a better compromise fitting all the cases.

Future perspective of this study, already proposed and faced by the researchers team of the University of Liege, is a highly coupled thermo-hydro-mechanical approach. In fact, one of the relevant properties of compacted bentonite is its

thermal behaviour, in particular its adequate thermal conductivity, necessary to prevent excessive thermal gradients induced by the nuclear waste.
Another important issue in the underground nuclear waste storage is the unavoidable presence of interfaces between different components, due to a logistic problem of placement. These interfaces play a crucial role given that they could represent a preferential path for both the groundwater and the radiotoxic nuclides, favouring thus their leak in the surrounding environment. In order to face this important issue, the analysis of the full scale problem would be required, as further prosecution of the study. In this application the hydro-mechanical behaviour of the compacted bentonite layer could be modelled by the calibrated Barcelona Basic model, which proved a satisfactorily predictive potential.

Acknowledgements

This work was conducted thanks to both the University of Liege and the Politecnico of Milano, which made their laboratories available; to the technicians who have helped me during the experimental test, to the students and the professors who have taught me how to manage a master thesis, and who have corrected my pages minutely. The biggest thanks goes to my friends, my boyfriend, my sister and my parents who have accompanied me through an intense five years path, and who have made it possible.

Bibliography

[1] AGI, 1994. *Raccomandazioni sulle Prove Geotecniche di Laboratorio.*

[2] Alonso, E.E., Gens, A., Josa, A., 1990. *A constitutive model for partially saturated soils*, Géotechnique 40, No. 3.

[3] ASTM, 2002. *Standard test methods for specific gravity of soil solids by water pycometer*, Designation D 854, ASTM International.

[4] Bishop, A. W., 1959. *The principle of effective stress*, Teknisk Ukeblad, 106(39).

[5] Carter, M., Bentley, S., 1991. *Correlations of soil properties*, Penetech Press Publishers, London.

[6] Controls Group, 2015. *General Catalogue.*

[7] Citrini, D., Noseda, G., 1987. *Idraulica*, Casa Editrice Ambrosiana.

[8] Daian, J.F., (2010). *Equilibre et transferts en milieux poreux I- Etats dequilibre*, HAL, open archives.

[9] Delage, P., Cui, Y.J., 2015. *Comportement mécanique des sols non saturés*, Techniques de l'Ingénieur, traité Construction, C 302.

[10] Delage, P., Cui, Y.J., 2015. *L'eau dans les sols non saturés*, Techniques de l'ingénieur Géotechnique.

[11] Dieudonné, A.C., Gatabin, C., Talandier, J., Collin, F., Charlier, R., 2016. *Water retention behaviour of compacted bentonites: experimental observations and costitutive model*, E-UNSAT 2016, Paris, Accepted for oral presentation.

[12] Dieudonné, A.C., Gerard, P., Collin, F., Charlier, R., 2012. *A Hydromechanical model for unsaturated bentonite incorporating the effect of microstructure*, 5^{th} International meeting, Montpellier.

[13] Dieudonné, A.C., Romero, E., Radu, J.P., Levasseur, S., Charlier, R., 2014. *On the role and influence of interfaces in underground disposals for nuclear waste*, 6^{th} Workshop of CODE-BRIGHT, Barcelone.

[14] Dieudonné, A.C., Talandier, J., Charlier, R., 2015. *On the modelling of compacted bentonite under in situ conditions.*

[15] Everett, D.H., Haynes, J.M., 1973. *Capillarity and porous materials: equilibrium properties*, Colloid Science 1.

[16] Fultz, B., Howe, J., 2013. *Transmission electron microscopy and diffractometry of materials*, Springer.

[17] Gatabin, C., Talandier, J., Collin, F., Charlier, R., Dieudonné, A.C., 2016. *Competing effects of volume change and water uptake on the water retention behaviour of a compacted MX-80 bentonite/sand mixture*, Applied Clay Science, 121-122.

[18] Gerard, P., Charlier, R., Barnichon, J.D., Su, K., Shao, J.F., Duveau, G., Giot, R., Chavant, C., Collin, F., 2008. *Numerical modelling of coupled mechanics and gas transfer around radioactive waste in long-term storage*, Journal of Theoretical and Applied Mechanics, Sofia, vol.38, Nos 1-2.

[19] Giesche, H., 2006. *Mercury porosimetry: a general (practical) overview*, Part. Part. Syst. Charact, 23.

[20] Goguel, J., Candès, P., Izabel, C., 1987. *Stockage des déchets radioactifs en formations géologiques. Critères techniques de choix de site*, Rapport du groupe de travail présidé par le professeur Goguel, Ministère de l'Industrie, des P. and T. et du Tourisme, France.

[21] Grim, R.E., 1953. *Clay mineralogy*, McGraw-Hill.

[22] Hatert, F., 2013. *Minéralogie et radiocristallographie*, Cours de sciences géologiques, ULG.

[23] Japan Atomic Energy Agency, 2007. McGraw-Hill.

[24] Karnland, O., Muurinen, A., 2002. *Bentonite swelling pressure in NaCl solutions - experimentally determined data and model calculations*, International meeting, Reims.

[25] Lancellotta, R., 2012. *Geotecnica*, Zanichelli.

[26] Magnan, J.P., 2015. *Description, identification et classification des sols*, Techniques de l'Ingénieur, traité Construction, C 208.

[27] Magnan, J.P., Mestat, P., 1991. *Lois de comportement et modélisation des sols*, Techniques de l'Ingénieur, traité Construction, C 218.

[28] Micrometrics, 1986. *Instruction manual multivolume pycnometer 1305.*

[29] Mitchell, J.K., Foga, K., 2005. *Fundamentals of soil behaviour*, John Wiley and sons.

[30] NAVFAC, 1986. *NAVFAC design manual 7.2.*

[31] Nuclear Energy Institute, 2016.

[32] Nova, R., 2002. *Fondamenti di meccanica delle terre*, McGraw-Hill.

[33] Peltier, R., 1969. *Manuel du laboratoire routier*, Dunod.

[34] Peron, H., Hueckel, T., Laloui, L., 2007. *An improved volume measurement for determining soil water retention curves*, Geotechnical Testing Journal, Vol. 30, No. 1.

[35] Pusch, R., 1979. *Highly compacted sodium bentonite for isolating rock-deposited radioactive waste products*, Nuclear Technology 45.

[36] Recherches et Realisations Remy, 2016. *3R Catalogue.*

[37] Romero, E., Gens, A., Lloret, A., 1999. *Water permeability, water retention and microstructure of unsaturated compacted Boom clay*, Engineering Geology 54.

[38] Romero, E., 2013. *A microstructural insight into compacted clayey soils and their hydraulic properties*, Engineering Geology 165.

[39] Ross, C.S., Hendricks, S.B., 1945. *Minerals of the montmorillonite group: their origin and relation to soils and clays*, Professional Paper 205-B.

[40] Samuels, S.G., 1950. *The effect of base exchange on the engineering properties of soils*, Building Res. Station Note No. CI 76 (Watford).

[41] Saba, S., Delage, P., Lenoir, N., Cui, Y.J., Tang, A.M., Barnichon, J.D., 2014. *Further insight into the microstructure of compacted bentonite-sand mixture*, Engineering Geology 168.

[42] Santucci De Magistris, F., 1996. *Comportamento di un limo sabbioso ed argilloso costipato ed addizionato con bentonite*, Doctoral thesis.

[43] Schaffer, M.B., 2011. *Toward a viable nuclear waste disposal program*, Energy Policy, 39.

[44] Shroff, A.V., Shah, D.L., 2003. *Soil mechanics and geotechnical engineering*, A.A. Balkema Publishers, Tokyo.

[45] Skartlatidou, A., Cheng, T., Haklay, M., 2012. *What do lay people want to know about the disposal of nuclear waste? A mental model Approach to the design and development of an online risk communication*, Risk analysis, Vol. 32, No. 9, 2012.

[46] Skempton, A.W., 1953. *The colloidal 'activity' of clays*, Proc. 3rd Int. Conf. Soil Mech.

[47] Stepkowska, E.T., 1990. *Aspects of the clay/electrolyte/water system with special reference to the geotechnical properties of clays*, Eng. Geol. 28 (3-4).

[48] Taborda, R., López, J., Bileak, J., 2012. *Nonlinear soil effects in large-scale 3D ground motion simulations*, Parallel Data Lab.

[49] Tang, A.M., Cui, Y.J., 2005. *Controlling suction by vapour equilibrium technique at different temperatures, application to the determination of the waterretention properties of MX-80 clay*, Canadian Geotechnical Journal, Vol. 42, No. 1.

[50] Terzaghi, K., 1943. *Theoretical soil mechanics*, John Wiley and sons.

[51] Tropeano, G., 2014. *Prove di laboratorio per la determinazione delle proprietà idrauliche e meccaniche dei terreni.*

[52] ULG Researcher Team, 2009. *Didactitiel de Lagaprogs.*

[53] USDA-SCS, 1990. *Elementary Soil Engineering*, Engineering Field Manual, Ch.4.

[54] Varma, R.S., 2002. *Clay and clay-supported reagents in organic synthesis*, Tetrahedron 58.

[55] Villar, M.V., 2004. *Thermo-Hydro-Mechanical Characteristics and Processes in the Clay Barrier of a High Level Radioactive Waste Repository. State of the Art Report*, Informes Técnicos Ciemat 1044.

[56] Wang, Q., Tang, A.M., Cui, Y.J., Delage, P., Gatmiri, B., 2012. *Experimental study on the swelling behaviour of bentonite/claystone mixture*, Engineering Geology 124.